JOURNAL OF MATERIALS SCIENCE **37** (2002) 2379–2405

Review
Progress in Ostwald ripening theories and their applications to the γ'-precipitates in nickel-base superalloys

Part II *Nickel-base superalloys*

A. BALDAN
Department of Metallurgical and Materials Engineering, Mersin University, Çiftlikköy/Mersin, Turkey
E-mail: abaldan@mersin.edu.tr

The Lifshitz-Slyozof-Wagner (LSW) theory, which corresponds to a zero volume fraction approximation, was developed to model kinetics of precipitate growth from supersaturated solid solutions. The subsequent modifications of the LSW theory for the incorporations of various factors including volume fractions of precipitates to fit the experimental data from the coarsening precipitates were made by various workers during last twenty five years. The LSW theory and its modifications have been applied on the diffusion-controlled Ostwald ripening of the γ' precipitate particles [Ni_3(Al,Ti)] in nickel-based superalloys. The important Ostwald ripening theories were reviewed in the part I of this paper, and the coarsening characteristics of the γ'-precipitates in Ni-base high temperature superalloys are presented in detail in relation to these theories in the present part. A model developed by D. McLean can be used to predict the γ'particle growth over service lifetimes in the case of relatively Al-rich nickel-base superalloys. Additional fundamental data (such as the precipitate-matrix interfacial energy, diffusivity of the component species of the particle, and the equilibrium solubility with a particle in nickel-based superalloys) can be obtained from experimental results for coarsening, if the concentration changes during coarsening can be measured precisely, using the methods developed by A. J. Ardell. Furthermore, the factors affecting the shape changes and splitting of the γ' precipitate particles during the coarsening were also considered seperately since the classical Ostwald ripening theories can not explain the morphological changes.

1. Introduction

Nickel-base superalloys are widely used in applications requiring strength at high temperatures. Most of these alloys are precipitation hardened by a Ni_3(Al, Ti) γ' phase which has an ordered fcc structure ($L1_2$-type) and precipitates coherently in a nickel-rich fcc matrix. The strength of a given alloy is dependent upon such factors as volume fraction, particle size, coarsening rate, and composition of γ' phase. All of these factors can be controlled to varying degrees by heat treatment. Their strength derives mainly from the precipitation of the hard, ordered γ' phase dispersed throughout the material. Information on the influence of time and temperature on the γ' precipitate would be valuable not only in the design of heat treatments for commercial superalloys but also for understanding the effects of high service temperatures where coarsening and perhaps partial solutioning of the γ' phase occur. The initial heat treatment of the alloy and its subsequent thermal aging conditions under which these materials are formed greatly affects the size, shape, distribution and volume fraction of the γ' second phase particles and in turn essentially determines the properties of the alloy.

The changes in the shape and size distributions of the constituent phases which occur at elevated temperatures by diffusion can be either beneficial or detrimental [1, 2]. Growing demands both for improved materials through process optimization and for more effective use of existing materials by reliable life-prediction techniques have emphasized the need for better quantitative descriptions of the processes leading to morphological changes (instabilities) in alloy systems [1–5].

The following factors affect the shape changes of particles [6]: (a) the elastic energy, (b) volume fraction of particles, (c) elastic anisotropy, (d) misfit between particles and matrix, (e) plastic deformation, (f) applied stress, and (g) crystallographic orientation. γ'-particles in nickel-base superalloys generally change shape during coarsening. The fact that the interfacial energy provides a driving force, F, for the microstructural

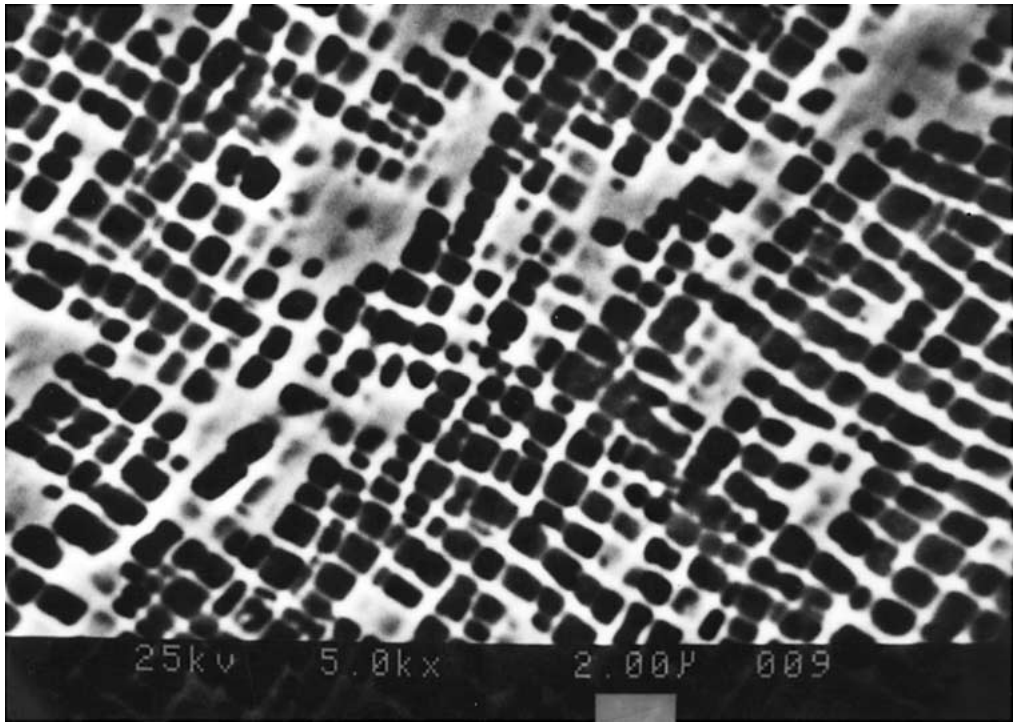

Figure 1 Rounded cuboidal type γ' particles in IN-100 alloy.

instability indicates the importance of the interfacial energy to control the microstructure. The energy associated with the coherency straining of the lattice due to coarsening has a minimum in the directions of lowest Young's modulus (i.e. along the ⟨100⟩ directions [7–9]. Consequently, there is a low strain energy associated with γ/γ' interfaces lying on {100} planes. It has been known [7, 10, 11] for many years that γ' precipitates in nickel-base superalloys change shape as they grow. Small precipitates are spherical when their diameters are less than 10 nm. As their size increases they become cuboidal, i.e. they acquire segments of flat interfaces parallel to ⟨100⟩, so that their overall appearence resembles a cube with rounded corners (Fig. 1).

The past experiments have demonstrated that external stresses can significantly change the morphology of the precipitates and their spatial arrangements [12–15], resulting in so-called rafted microstructures consisting of alternating lamellae of γ and γ' phases (14). Such-raft-like structures can improve the yield strength by about 30% and prolong the creep rupture life for four times as compared to those without rafting [16].

McLean [17] distinguished two broad categories on the basis of the origins of the driving forces for the instabilities, i.e., intrinsic and extrinsic instabilities. The motivation for intrinsic instabilities results from the reduction in free energy as the isolated alloy tends towards thermodynamic equlibrium. Interfacial energies make a particularly important contribution to this group, leading to, for example, particle coarsening. Because the driving force for precipitate coarsening comes from the specific free energy of the precipitate/matrix interface, low growth rates demand that the γ/γ' interfaces be coherent and have a low lattice mismatch.

The microstructural changes leading to a reduced free energy, which occur in isothermally annealed complex polyphase alloys in the absence of external stress influences (intrinsic instabilities), take a variety of forms. The most important in the total interfacial energy of the system is a reduction in the area of various interfaces (e.g. grain boundaries, precipitate boundaries, etc.). This effect is manifested in the following ways [1]: (a) grain or precipitate coarsening (e.g. grain growth, Ostwald ripening), (b) shape changes of grains or precipitates (e.g. spheroidization, faceting, agglomeration etc.), and (c) interaction of phase or grain boundaries.

Coarsening is usually found to follow the behaviour predicted by one of two models: diffusion-controlled or interface-controlled coarsening. As far as the author's knowledge no study to date has shown strong evidence for interface-controlled coarsening in nickel-base superalloys, so this model will not be discussed.

In the Part I of this work, the important aspects of the Ostwald coarsening theories including the Lifshitz-Slyozov-Wagner (LSW) theory and its modifications by various workers were presented, and in this part, the applications of these theories on the ripening characteristics of γ' precipitates in nickel-base superalloys will be discussed. Furtheremore, the shape changes and splitting of γ' particles under the various conditions will also be reviewed.

2. Nickel-base superalloys

Cast nickel-base superalloys are typically composed of high volume fractions of γ'-phase coherently precipitated in a fcc matrix, together with eutectic phases and one or more carbide phases. The desired properties and resistance to microstructural changes at high temperatures in these alloys are obtained by all phases with suitable structure, shape, size and distribution. It is widely regognized that coarse-grained with serrated grain boundaries, homogeneous compositions with uniform cubic $\gamma - \gamma'$ microstructures and small discrete phases at grain boundaries are typical microstructural

features in modern advanced nickel-base cast superalloys [1–3]. Among all the microstructural factors, the γ' precipitate morphology plays an important role in influencing the properties of nickel-base superalloys [18]. Therefore one subject which is important to the development of new types of superalloys is how to produce the desirable γ' precipitate morphology. Since such precipitate particles can grow during the initial heat treatment, it is very important to be able to predict the kinetics of growth and subsequent behaviour of this precipitate phase [19, 20].

The $\gamma - \gamma'$ microstructure of some nickel base superalloys can undergo drastic changes during high temperature heat treatments. The morphology of the γ'-precipitates evolves from different mechanisms [21]: (a) competitive coarsening in order to reduce the specific area of the $\gamma - \gamma'$ interface (Ostwald ripening) [i.e. 19, 22–25], and (b) shape changes in order to minimize the sum of interfacial and elastic interaction energies. Research works have been conducted concerning the coarsening of the γ'-precipitates during high temperature exposures of the alloys (see for example [26–28]. It has been observed that in general the precipitates grow at an almost constant volume fraction, following a $(\text{time})^{1/3}$ power law concerning diffusion-controlled particle coarsening in agreement with the LSW theory.

Precipitation in Ni-base superalloys generally occurs by a classical nucleation and growth mechanism with a precipitate sequence of: *spheres* → *cubes* → *plates.* The γ' precipitates are believed to nucleate as spheres to minimize the surface area/unit volume. As the particles grow, the coherency strains increase and thus the reduction in strain energy more than compensates for the increase in surface area/unit volume manifested as phase migration, coarsening, and shape changes, caused by diffusion along the applied potential fields.

Lattice-parameter mismatch $\lfloor \delta = 2(a_{\gamma'} - a_\gamma)/(a_{\gamma'} + a_\gamma) \rfloor$, where $a_{\gamma'}$ and a_γ are the lattice parameters for the γ' and γ phases, respectively, influences the γ' particle size at which this transition occurs [29], as shown in Table I [26] and must be greater than 0.1% at the aging temperature in order for cubes to form [22]. A study of Table I reveals that larger mismatch causes the transition to occur at smaller sizes. However, the sign of mismatch apparently does not affect this transition strongly [26].

As the particles continue to grow, they almost always align along ⟨001⟩ directions due to elastic interactions between particles [22, 30, 31]. It appears as though the elastic interactions that induce alignment determine which particles will coarsen, but not the rate at which they do so [22]. Interestingly, this alignment would probably not occur if the interfacial energy were not so low, since capilarity would overhelm the effects of elastic interaction [29]. Relative orientations between particles would then have little influence in determining which particles coarsened [22].

TABLE I Effects of lattice-parameter mismatch[a], δ upon shapes of γ' [26]

Alloy	Room-temperature misfit (%)	Size at which γ' shows significant departures from spherical shape (microns)
1. Udimat 720	<0.02	0.7
2. Nimonic 105	−0.04	0.7
3. Experimental alloy	−0.11	
4. Nimonic 115	−0.18	0.5
5. Nimonic 80A	+0.32	0.3
6. Nimonic 90	+0.34	0.3

[a] $\delta = 2(a_{\gamma'} - a_\gamma)/(a_{\gamma'} + a_\gamma)$.

It is widely known that the γ' precipitate in the Ni-Al system undergoes a succession of morphology changes as it grows. In order to minimize surface energy, the initially observed shape is sphere. As the precipitate grows the misfit strain energy continues to increase so that gradually a cuboidal and then cube morphology best minimizes the total energy of the precipitate. Many researchers have observed this continuing change using TEM [7, 26, 32–35] and have observed the γ' cubes to be aligned parallel to the ⟨100⟩ directions in Ni after prolonged aging. The elastic modulus for nickel is minimum along the cube directions so this orientation of the precipitates is to be observed. Thereafter at much larger sizes more complicated structures occur.

2.1. Effects of γ' morphology on the creep resistance of nickel-base superalloys

Mechanical properties of Ni-based superalloys are strongly affected by the morphology, distribution, and size of γ' precipitates in the γ matrix. The strength of superalloys is related to the interactions between γ' particles and moving dislocations. During the creep exposure, γ' ripening can take place and the particles may remain equiaxed [28], become irregularly shaped [2, 36, 37] or corsen into rod or rafted morphologies [2, 3, 12, 38–40].

The creep resistance of Ni-base superalloys depends critically on the size and spacing of the γ' precipitates. Using IN-100 it was concluded [1] that the creep strength in terms of minimum creep rate is predominantly governed by γ' size, density and shape of particles, and to a lesser extent by the cubic particles alignment along the ⟨100⟩. The initial γ' precipitate morphology in cast IN-100 is usually in the form of cubes or spheres, depending on the misfit parameter between γ' and γ matrix [41]. The strengthening contribution of γ' in this alloy is partly dependent on the size, spacing, shape and volume fraction of the particles [1]. The strong dependence of creep rupture life on the γ' volume fraction has been observed in the past [1, 2, 42, 43]. The highest creep rupture life [1] was achieved at ≈50 vol% γ'. In a previous work [43] using alloys with compositions near Nimonic 80A, a good correlation was obtained between creep strength and the cube root of the γ' volume fraction. Caron and Khan [44] have shown the benefits of optimizing the microstructure for the single CMSX-2, which seems to be associated with the regularity of γ' distribution rather than of size, and considerable interests has also been shown in producing rafts of γ' in some single crystal alloys [45] to improve the creep performance. However, McLean [46] pointed out that all of these factors

produced relatively small benefits compared to the γ' volume fraction effect.

One of the most important characteristics during high temperature creep of single crystal nickel based superalloys is the rapid directional coarsening of the cubic N_3Al (γ') precipitates to form preferentially orientated rafts. Directional coarsening of the γ' precipitates under the action of an applied stress was first studied in detail by Tien and Copley [12], and this phenomenon has subsequently been observed in many experimental and commercial single crystal nickel based superalloys, and the morphology and the size of the γ' rafts have been widely studied [47–50]. Some papers are devoted to analysing the magnitude and distribution of the misfit stress by using fine element methods [50, 51].

3. Shape changes in γ' particles: factors affecting the shape changes

It is worth mentioning that several experimental studies have shown that a uniaxial stress applied during precipitation can alter the precipitate morphology [2, 12, 38, 52]. Tien and Copley (12) have studied ⟨100⟩ oriented single crystals of Udimet 700. After stress-free annealing this Ni-base superalloy contains coherent cube-shaped $\gamma'(Ni_3TiAl)$ particles. The misfit (δ) between the γ' particles and the matrix results in a pure dilatation. Tien and Copley found both tensile and compressive stress applied at elevated temperatures lead to unidirectional coarsening followed by agglomaration of the γ' precipitates. In the case of tensile stress annealing, γ' precipitate plates form with their broad faces aligned perpendicular to the stress axis. On the other hand, compressive stress gives rise to needles aligned parallel to the stress axis.

3.1. γ' shape change in absence of applied stress

Although there have been many studies on the morphology and evaluation of coherent precipitates in the absence of external stresses [13, 14, 53–57], the studies on the effect of applied stress on the particle morphology and the evolution kinetics are much fewer. Most of the previous studies were conducted for a single isolated particle in an infinite matrix using Eshelby's method [8, 58]. The particle-particle interactions were not taken into account, which is important when the volume fraction of the precipitate phase is high. In addition, the previous studies were mainly concerned with the equliubrium shape of a particle rather then its evolution path although most experimentally observed particle shapes are most likely nonequilibrium. In order to incorporate particle-particle interactions and investigate the evolution of particle morphologies, a number of simulation models were developed, including the Monte Carlo method, continuum model, and atomistic approach [59–61]. However, all these methods did not take into account the possibility of several degenerate ordering states, or orientations, and hence, may be applied only to the systems with iso-structural phase seperation such as spinodal decomposition.

In their computer simulation of the microstructural evalution during precipitation of γ' particles in the absence of applied stresses Li and Chen [62] showed that a grown γ' particle exhibits a cuboidal shape with its $\{100\}\gamma'$ plane parallel to $\{100\}_\gamma$ plane of the matrix. Since γ/γ' interfacial energy was assumed to be isotropic, the cuboidal and the $(100)_{\gamma'} \| (100)_\gamma$ orientation relationship are therefore attributable to the elastic energy. The simulated morphology is consistent with the experimental observations [14] as well as previous theoretical calculations and computer simulations [13, 14, 53, 56]. It is generally agreed that the minimization of strain energy is mainly responsible for the morphology of a coherent precipitate, because the elastic energy is a function of the shape, orientation and volume of the precipitate, and the anisotropy of interfacial energy is small.

The morphology of a γ' particle in a multi-particle system is affected by its neighbor particles because of the elastic interaction between the γ' particles. When the two particles impinge, they may coalesce and form a single γ' domain, or they may stay separated by a thin layer of the matrix phase, depending on their ordering states, i.e. depending on whether or not they are in antiphase states. The morphological pattern of a multi-particle system is hence influenced by a number of factors, such as the density, mutual position, and the ordering states of γ' particles [62].

3.2. γ' rafting under applied stress

Rafting occurs by coalescence of the cubic γ' precipitates along the plane of the initially less highly stressed matrix channels. The channels along which coalescence occurs are generally devoid of dislocations. Once dislocations are introduced, directional coarsening occurs very rapidly, before complete relief of the misfit stress [51]. The applied stress, lattice misfit, and modulus mismatch provide the driving force for shape evolution and determine the orientation of the γ' rafts [53]. In another words, the driving force of the rafting of γ' precipitates is supposed to be the superimposing roles of the applied and coherent stress owing to the misfit between the γ and γ' lattice parameters [51, 63].

Under an applied stress at elevated temperatures, the discrete-type γ' particles link up to form a rafted γ' morphology. Different types of rod or rafted γ' morphologies may develop during creep deformation, which depends on the lattice mismatch, the sign of the applied stress and the crystallographic orientation [53, 64, 37]. Also depending upon relative elastic moduli and lattice-parameter mismatch of the two phases, the γ' particles may coalesce either into rods or plates parallel to the applied stress or into plates perpendicular to it (Fig. 2). The effects of rafting upon creep-resistance make it by far the more important of the two cases [29, 2].

The γ/γ' lamellae are believed to strengthen the material during creep, because this rafted morphology of the γ' phase essentially eliminates γ' particle bypassing [16, 42], which is the creep mechanism normally operative in conventional Ni-based superalloy at elevated temperatures and low stress [65, 66].

Some experimental observations have provided evidence that the internal misfit stress as well as the applied

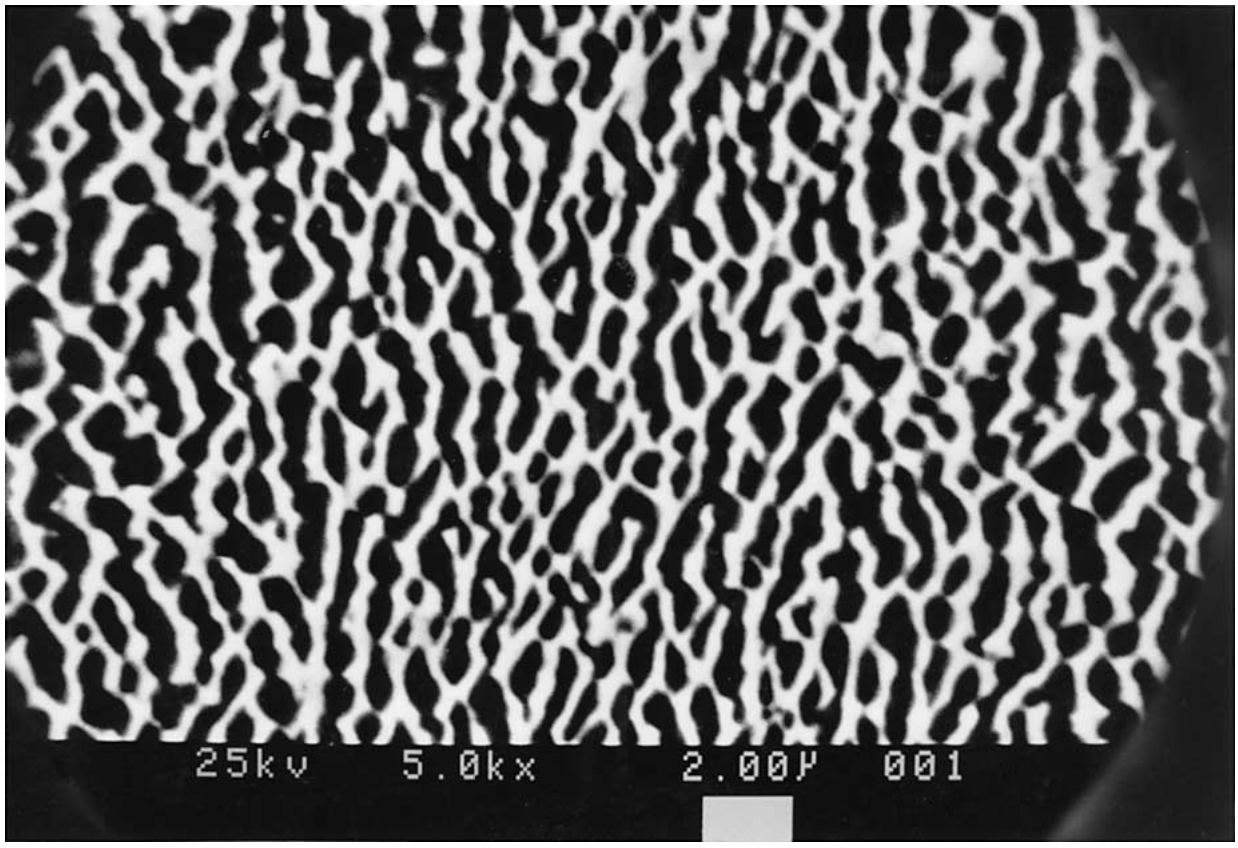

Figure 2 Coarsened and elongated (or rafted) γ' precipitate particles developed during the creep test at 1173 K/276 MPa for cast IN-100 alloy.

stress is important to the morphological evolution of the γ' rafted precipitates. For example, in a SC-83 single crystal superalloy after creeping at 600 MPa and 900°C [67] and SMSX-4 after creeping at 980°C and 350 MPa [68, 69] it has been shown that the γ' precipitates are linked to each other along the [010] orientation into rafted structures in a side cocavity mode. These results also show that the alloy composition, the applied stress, and temperature level have an important influence on the morphological evolution of the γ' rafts.

In studing the directional coaressening of the γ' phase, Tian *et al.* [70] have used two model single crystal nickel based superalloys, possesing a negative misfit ($a_\gamma > a_{\gamma'}$) under the different creep conditions. When the stress is applied on the single crystal alloy, an increased strain occurs in the matrix since the stiffness in the matrix is smaller than that of the γ' phase. A small elastic strain is produced in the $\langle 110 \rangle$ direction on the (001) crystal plane in the matrix since the $\langle 110 \rangle$ direction possesses a denser atom arrangement and a higher elastic modulus than the other. While the [100] and [010] directions possess the lowest elastic modulus as a result of a looser atom arrangement. Therefore, an elastic strain is easily produced in these directions under applied stress, which displays the anisotropy of the single crystal alloy. A schematic illustration of the coherent misfit at the γ'/γ interfaces is shown in Fig. 3. The cubic γ' phase is embedded in the γ matrix in aged condition, and there is the same gradient of coherency misfit γ'/γ interfaces for both horizontal and vertical channels, as shown in Fig. 3a. An approximate value of the misfit stress σ_{mis} is given by [49] $\sigma_{\text{mis}} = AE\delta$, where A is constant, E is the elastic modulus, and δ is the misfit in the alloy. When the tensile stress is applied, the lattices of the γ matrix in the horizontal channels are stretched along the [001] direction, and contrasted along the [100] and [010] directions (matrix bulk conservation). This reduces the misfit stress and the coherent strain at the γ'/γ interfaces normal to stress axis, and the zero misfit stress at the interfaces can be calculated under the action of the effective stresses [71]. By comparing the stress condition before and after deformation, the change of the coherent misfit stress gradient was shown to occur at the γ'/γ interfaces on the (001) crystal plane. In the mean time, the γ' phase near the interfaces is subjected to an extruding force owing to the contraction of the γ matrix.

Until recently, all theories of the driving force for rafting have considered the compositions of the two phases to be fixed, although accepting that the rate of rafting might be controlled by diffusion. Nabarro [63] has analyzed the chemical driving force in superalloys. His analysis in the elastic regime [e.g. 72, 73] rests on Eshelby's recognition that the thermodynamic presure on an interface has two components: (i) the difference in elastic energy densities across the interface, and (ii) the work done by the normal traction across the interface when the interface moves. Suppose a tensile stress σ is applied along a cube axis to a superalloy with a positive misfit, i.e. the lattice parameter of the γ' particles exceeds that of the γ matrix. There is a large increase in the energy density in the γ channels parallel to the applied tensile stress, because the material already has an internal stress in the same direction. There is also a first order increase in the work done by the traction across the transferce interfaces. These effects both

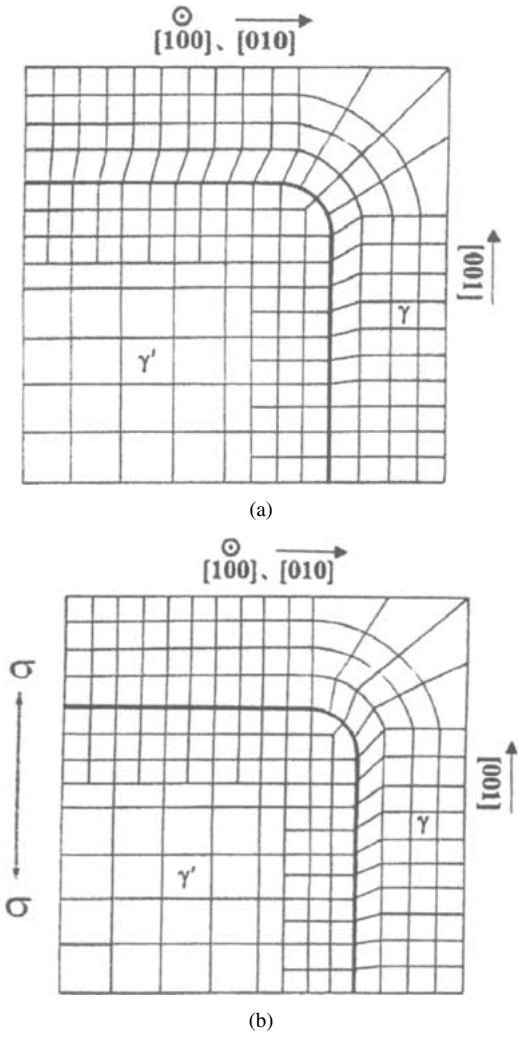

Figure 3 Schematic illustration [70] of lattice misfit at different crystal planes: (a) unstressed and (b) under applied stress. Note that due to symmetry only one quarter of precipitate and surrounding matrix is shown.

cause a thermodynamic pressure, tending to displace the corresponding interface from γ' towards γ. If the elastic constants of γ and γ' are equal, the two pressures are equal, and there is no tendency to rafting. If γ' has a higher elastic modulus, the elongation of the γ sheets parallel to the tensile axis is constrained, the additional thermodynamic pressure on the lateral interfaces is reduced, and rafting occurs by outward displacement of the transverse interfaces.

When plastic flow occurs, the difference in elastic constants become negligible. A high energy density builds up in the transverse γ sheets, and rafting occurs by outward motion of the transverse interfaces, reducing the volume which has a high energy density [63].

Microstructure of γ'/γ superalloy may be dramatically changed by applied constraint-strains. Using the computer simulation of the microstructural evolution, it was demonstrated by Li and Chen [62] that γ' domains were elongated along the applied tensile strain and formed a raft-like microstructure. In order to explain the rafting of γ' phase, they used the effective eigen-strain which corresponds to the effective stress. In the absence of the applied strain, the eigen-strain is dilatational strain, which results in a cuboidal morphology of the γ' phase. When the uniaxial strain is applied along the y axis, it results a tetragonal growth of the γ' phase with elongation along y axis, leading to the minimum increase in the elastic energy. An compressive strain, hovewer, results the higher strain along the x-direction than that of y-direction (applied strain direction) and this makes the γ' phase elongated in the direction perpendicular to the constraint strain. This simulated rafting arrangement and its correlation with the applied strains were consistent with experimental observations [14].

3.3. Elastic energy consideration

3.3.1. Introduction

Precipitate misfit (stress-free transformation strain) is known to be a critical factor in determining the morphology of isolated precipitates [74–76] and the stability of two or more precipitates against coarsening [7, 77–79]. The coherency strains associated with the misfit result in an elastic interaction between precipitates. The sign and magnitude of the interaction energy is a complicated function of precipitate size, morphology, elastic constants and the intercenter distance and orientation between the precipitates. Under certain physical conditions the sign of the interaction energy may be negative, implying that system elastic energy can be decreased by aligning the precipitates in a certain orientation at a certain distance of separation. If the magnitude of the elastic interaction is large enough, total system energy may be minimized by retaining a certain number of precipitates. This stabilizes the precipitates against coarsening.

Both the elastic and interfacial energies of a precipitate embedded in a solid matrix depend on the precipitate shape. The morphology that minimizes the elastic energy may be different from that which minimizes the interfacial energy. Since the ratio of elastic to interfacial energy is proportional to precipitate size, the particle possesing minimum energy should tend toward the shape corresponding to the minimum interfacial energy shape when the particle is small and the minimum elastic energy shape when the particle is large.

The elastic interaction energy between precipitates is of great interest in connection with precipitate alignment during coarsening. Although there have been many studies on this subject, most of the works have been limited either to a homogeneous case [74, 80–82] wherein the elastic constants of the precipitate and matrix phases are assumed to be equal, or if inhomogeneous to isotropic elasticity [7, 74, 83, 84]. By inhomogeneous it is here meant that the elastic constants of the precipitates and matrix are not the same. However, most phenomena caused by elastic interactions are observed in anisotropic materials with different elastic constants for the matrix and precipitates.

3.3.2. Theoretical background

Several thoretical models which treat the change in elastic energy with particle shape have been published (see for example [12, 39, 40, 53, 85]). In the discussion of their observations, Tien and Copley [12] gave only a qualitative analysis and could not draw quantitative conclusions regarding the influence of the elastic energy

on particle shape. A second set of calculations given by Cahn and Weins [39] is more comprehensive. These authors invoked only the variation in external work done on the system and neglected the variations in stored elastic energy. Moreover, Cahn and Weins used an approach which assumes that stresses and strains are uniform both inside the particles and matrix. Sauthoff [40] used the results of the Eshelby's theory, but took into account only the inclusion effect neglecting other terms. Moreover Sauthoff developed his analysis for the case where the misfit is a tetragonal distortion and not a pure dilatation.

Pineau [53] studied the influence of uniaxial applied stress on the morphology of coherent precipitates during ripening by using the Eshelby's theory of inclusions and inhomogeneities. In this work he calculated the three components of elastic energy. Then the results of these calculations were used in discussing the influence of the ratio between the Young's modulus of the precipitates (E_p) and that of the matrix (E_m), the misfit parameter (δ) and the applied stress (σ_A) on the particle shape. In this study it is assumed that the volume fraction is constant and sufficiently low so that the elastic interactions between particles can be neglected. As shown by Eshelby [74], the variations in total elastic energy per unit volume (E_t) includes three terms [53]:

$$E_t = E_{\text{incl}} + E_{\text{int}} + E_{\text{inh}} \tag{1}$$

Where E_{inh} is the elastic energy for the inhomogeneity effect due only to the fact that, in the absence of coherency misfit arising from the differences of elastic constants between the particles and matrix. E_{incl} is the elastic energy for the inclusion effect which is related to the misfit. E_{int} is the interaction energy due to coherency stresses under an external applied stress. Considering the case when the matrix and particles have the same elastic constants. Eshelby [74] showed that the variation of the total energy of the system can be written $E_t = E_{\text{inc}} + E_{\text{int}}$. Tanaka *et al.* [86] extended the formalism by Eshelby to the case where the elastic constants of the matrix and precipitate particles are different. They showed that the variation in energy can be written as in Equation 1, as a sum of three terms

$$E_{\text{inl}} = (-1/2)\sigma^I_{ij} e^T_{ij}; \qquad E_{\text{int}} = -\sigma_A e^T_{33};$$
$$E_{\text{inh}} = (-1/3)\sigma_A e^{Th}_{33} \tag{2}$$

σ_A: applied stress ($\sigma_A > 0$ for a tensile stress; $\sigma_A < 0$ for a compressive stress). e^T_{ij}: transformation strains for the inclusion effect.

In dilatation case considered, $e^T_{11} = e^T_{22} = e^T_{33}$, $\delta = (a_p - a_m/a_m)$, where a_p and a_m are the lattice parameters of the precipitate particles and of the matrix, respectively, and $e^T_{ij}(i = j) = 0$. σ^I_{ij} : stress inside the inclusion in the absence of applied stress to the specimen. These stresses are determined from e^T_{ij} using Eshelby's method. e^T_{33}: "equivalent" strains for an inhomogeneous inclusion, i-e an inclusion with elastic constants different from those of matrix. These strains are also deduced from e^T_{ij}. e^{Th}_{33}: "equivalent" strains for an inclusion equivalent to the inhomogeneity. The equivalence was defined by Eshelby [74].

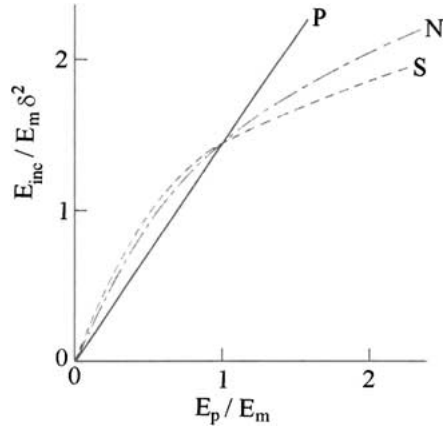

Figure 4 Variation [53] of the elastic energy for the inclusion effect (E_{inc}) with the ratio of Young's modulus of the precipitates and that of the matrix (E_p/E_m), δ is the misfit between the particles and the matrix. P, S and N refer to plates, spheres and needles, respectively.

Using the Pineau [53] analysis, the variation of E_{inl} with E_p/E_m is plotted in Fig. 4 for the three particle shapes: plates; spheres; and needles. The results are in agreement with those given by Robinson [87] who gave an exact solution to the elastic energy for the problem of ellipsoidal inclusions with different aspect ratios. It should be noted for $E_p = E_m$, the elastic energy is independent of the particle shape, as emphasized by Eshalby [8, 74]. Morover, when the elastic constants of the precipitates are different from those of the matrix, an interesting behaviour is observed. For $E_p/E_m < 1$, plates are the most stable, while for $E_p/E_m > 1$, the most stable shape corresponds to spheres.

Concerning the γ/γ' system where E_p/E_m is likely less than 1, several authors [7, 88] have observed that during stress-free coarsening large γ' particles align and agglomerate to form shapes which is approximately considered as plates. However, as pointed out by Eshelby in the study published by Ardell and Nicholson [7], other effects such as local elastic interactions between neighboring particles can intervane.

According to Pineau's calculation for UDIMET 700 alloy $E_p/E_m \cong 0.8$. Taking also $\sigma_A/E_m = \pm 10^{-3}$ and $\delta = +2 \times 10^{-4}$ which correspond approximately to the values used by Tien and Copley [6], a value of $\sigma_A/E_m\delta = \pm 5$ was found. As a result of this calculation, Pineau [53] has shown that a tensile stress gives rise to plate perpendicular to the stress axis, while a compressive stress leads to needles aligned with the stress axis. These predicted shape changes are in agreement with those observed in UDIMET 700 [52].

From the Pineau's work the following conclusions can be made: (a) when $E_p = E_m$ the particle shape is neither influenced by the applied stress nor by δ. This result is well known and was emphasized by Eshelby [8, 74]; (b) for large applied stresses and or low δ the inhomogeneity effect is the most important. Plates perpendicular to the stress axis are elastically the most favorable. This result agrees with the theoretical analysis by Tien and Copley [12]; (c) when a moderate stress is applied an interesting influence of E_p/E_m is observed. In the case where $E_p/E_m < 1$ and if, for instance $\delta > 0$, a tensile stress always favors the plate shape, while a compressive stress first favors the needle shape

and then, for higher stresses, the plate shape again. In the case where $E_p/E_m > 1$ and $\delta > 0$, there is a large range of applied tensile stress where the spherical shape leads to the lowest elastic energy.

Carry and Strudel [65, 89] investigated the coarsening under stress of a nickel-base alloy which contains γ' particles with $\delta > 0$. They showed that under a tensile stress the γ' precipitate agglomerate into needle shape particles aligned with the tensile axis, while a compressive stress favors plates perpendicular to the stress axis. This situation, which is the reverse of that found in Udimet 700, is in agreement with the behaviour predicted by Pineau [53] for moderate values of the applied stress.

Following the difference method of Eshelby [7], Johnson and Lee [9] studied the elastic interaction energy between two spherical precipitates embedded in an infinite matrix of cubic anisotropy as a function of their distance of seperation and alignment direction.They considered two separate systems: one consisting of two misfitting inclusions surrounded by an infinite matrix while the other is composed of two misfitting inhomogeneities. Since the total elastic strain energy of each system may be writen [9]:

$$E' = E'_{\text{self}} + E'_{\text{int}} \tag{3}$$

where E'_{self} is the self energy which is independent of the relative positions of the two precipitates, and E'_{int} the interaction energy. and,

$$E = E_{\text{self}} + E_{\text{int}} \tag{4}$$

Where E' is the total energy of the system containing the two inclusions, with the meaning of the other terms self-manifest. Subtracting Equation 4 from 3:

$$E' - E = E'_{\text{self}} - E_{\text{self}} + E'_{\text{int}} - E_{\text{int}} \tag{5}$$

or

$$\Delta E = \Delta E_{\text{self}} + E'_{\text{int}} - E_{\text{int}} \tag{6}$$

Rearranging Equation 6 for E'_{int}, the interaction energy between two misfitting inhomogeneities gives:

$$E'_{\text{int}} = \Delta E - \Delta E_{\text{self}} + E_{\text{int}} \tag{7}$$

Therefore, E'_{int} can be determined if one can obtain ΔE, the difference between the total elastic strain energies for the two systems, ΔE_{self}, the change in self energy, and E_{int}, the interaction energy between the two homogeneous inclusions.

Using the above analysis [9], Fig. 5 was ploted in which the interaction energies are compared as a function of distance, R' in a Ni matrix in the [100], [110], and [111] directions, respectively. Attractive interaction along the [100] direction for Ni and Cu matrix should be expected on the consideration that the [100] direction is the elastically soft direction for cubic materials in which the anisotropic factor, $H(=2C_{44} + C_{12} - C_{11})$, is positive. On the other hand, the [100] direction is elastically hard [90] and thus should show a repulsive interaction for the prepitates positioned in this direction.

Ardell [7] analyzed the elastic interaction of γ' precipitate particles in γ with the isotropic assumption. Although the actual shape of γ' particles is a cuboid, on the basis of an isotropic, spherical precipitate assumption, they predicted that the [100] alignment of γ' particles in Ni-6.71 wt% Al alloys is due to the elastic interaction. The isotropicity argument [91] shows an an attraction when $\Delta E = E_p - E_m$ is negative as in the case of γ' in γ. However, the isotropicity argument can predict neither a stable configuration nor the particular orientation relationship. A simple monotonic attractive force can not cause a stable configuration for particles because they should attract each other until they contact and thus coarsen [9]. On the other hand, from the Johnson and Lee's [9] results based on the anisotropic elasticity, though it is also assumed spherical shapes rather than cuboidal shapes, the [100] alignment of the γ'-phase particles (Ni_3Al) is correctly expected. In Fig. 5, the [110] and [111] alignments show a repulsive

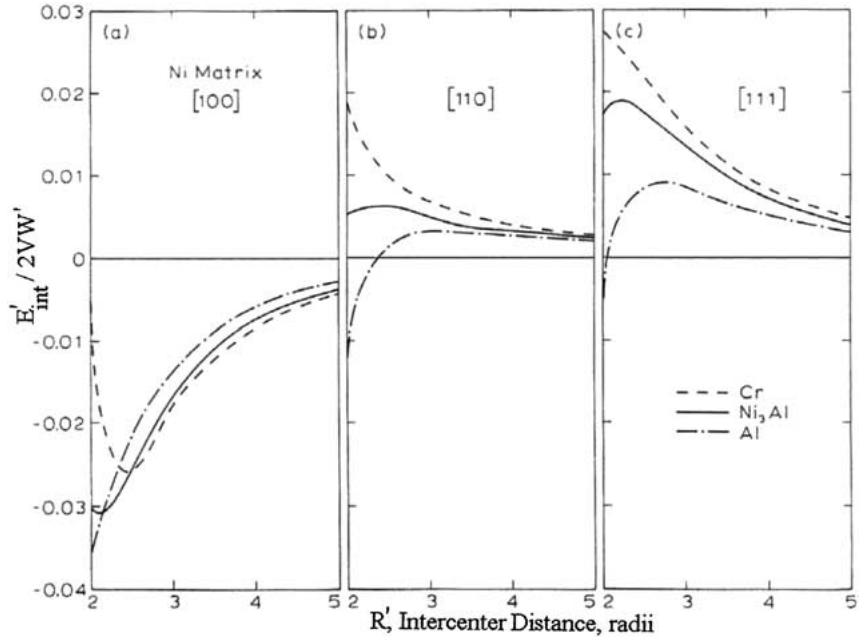

Figure 5 Elastic interaction energy [9] for two spherical precipitates as a function of distance, R', in a Ni matrix aligned along: (a) [100], (b) [110], and (c) [111] directions. Note that W' is the strain energy per unit volume for an inhomogeneous case associated with a spherical precipitate in an infinite matrix, and V is the volume of the system.

interaction, but the [100] alignment for the Ni_3Al precipitates in Ni exhibits an attractive one with minimum value at $R' \cong 2.1$ (where R' is of the intercenter distance between particles). The strength of the elastic interaction was also estimated by Ardell *et al.* [7]. Based on the isotropic elasticity assumption, they showed that the minimum radius of γ'-particles necessary to break even with thermal fluctuation at 700°C is approximately 100 Å. Using the Ardell *et al.* work at $R' = 2.1$ for the [100] alignment of Ni_3Al particles, Johnson and Lee [9] estimated the minimum radius to be about 20 Å, which is necessary to stabilize the γ'-particles against thermal fluctuation.

Therefore, the prediction made by Johnson and Lee [9] showed that the analysis of the elastic interaction of γ' particles in γ-matrix, in terms of anisotropic elasticity, show that the [110] alignment yields an attractive interaction with its maximum values at a distance slighly larger than the particle diameter. These results confirm the experimental observations of the [100] alignment of γ'-particles in Ni-base superalloys [12], though a spherical shape rather than a cuboid is assumed in the analysis. It was also found that the strength of the elastic interaction is quite stronger than Ardell *et al.* result [7] based on the isotropic assumption. The reason [9] is that when the particles are far apart, the interaction energy, E'_{int} varies as R'^{-6} for the isotropic case, but as R'^{-3} for the anisotropic case, where R' is the distance between precipitate paricles.

Johnson [85] investigated the stability against coarsening of two misfitting spherical precipitates subjected to an applied uniaxial tensile stress. In this work, regions and conditions of precipitate stability were determined and relationships between surface energy, matrix and precipitate elastic constants, precipitate misfit and applied stress were obtained. The bifurcation approach was shown to be a powerful tool in examining the stability of elastically interacting precipitates. In this analysis, the total system energy was calculated using the following expression [85]

$$E^T = E_{\text{el}} + E^M_{\text{int}} + E_a + E^A_{\text{int}} + E_s + E_{\text{pot}} \quad (8)$$

where E_{el} is the elastic self-energy of each precipitate in the absence of an applied stress, E_s is the surface energies associated with each precipitate-matrix interface, E^M_{int} is the interaction energy between precipitates arising from the coherency strains, E_a is the interaction energy between each precipitate and in the presence of an applied stress field, E^A_{int} is an interaction energy between precipitates arising from the applied stress field, and E_{pot} is a change in the potential energy of the loading mechanism that can be shown to depend upon the internal stress.

Precipitate stability thus requires that a variation in E^T with respect to mass exchange be greater than or equal to zero, i.e. the system energy is a relative or absolute minimum. In the absence of an applied stress field, system energy [see Equation 8] is expressible as [85]

$$E^T = E_{\text{el}} + E^M_{\text{int}} + E_s \quad (9)$$

The terms are in independent of the relative orientations of the precipitates. If the particles are constrained to remain spherical $R \equiv (r_1 - r_2)/(r_1 + r_2)$ can be used to describe the relative sizes of the two particles. Here r_1 and r_2 are the radii for precipitates 1 and 2, respectively. As R defines the distribution of mass between the two particles, stable solutions are determined from the extrema of Equation 9 with respect to R. Normalizing E^T by $3\,\phi\beta/4\pi$, (which does not affect stability calculations since the volume fraction of the second phase particle ϕ is held constant and β is a function of system elastic constants and precipitate misfit), differentiating with respect to R and setting the derivative $\mathrm{d}E^T/\mathrm{d}R$ equal to zero gives [85]

$$0 = \frac{2R(R^2-1)}{(1+3R^2)^{5/3}}[-Z + M(R,d)] \quad (10)$$

where $M(R,d)$ is a complicated function of R and d [85], where $d = R'/(3\phi/\pi)^{1/3}$ and R' is the distance between the centers of the two spheres. Johnson [85] has introduced a dimensionless parameter Z such that

$$Z = \frac{-4\pi\psi_{\text{int}}}{\beta}\left(\frac{8\pi}{3\phi}\right)^{1/3} \quad (11)$$

where ψ_{int} is the surface energy per unit area. E_{el}, being independent of R, makes no contribution to Equation 10. Thus the extramizing solutions to Equation 10 are

$$R = 0 \quad (12a)$$

$$R = \pm 1 \quad (12b)$$

$$M(R,d) = Z \quad (12c)$$

When the applied stress is assumed to be a uniaxial tensile stress, two parameters determine the stability of the precipitates for a given distance of separation, R', the relative sizes of the precipitates, R and their orientation with respect to the applied stress. Thus, in seeking extramizing solutions of the system energy, the following two conditions must be satisfied,

$$\frac{\partial E^T}{\partial R} = 0; \qquad \frac{\partial E^T}{\partial X} = 0 \quad (13)$$

where

$$E^T = E_a + E^A_{\text{int}} + E_s + E_{\text{pot}}$$

and $X = \cos(\theta)$ has been chosen as the parameter defining the relative orientation of the precipitates with respect to the applied uniaxial tensile stress. Here θ is defined as the angle between the line joining the centers of the two precipitates and the direction of the applied uniaxial tensile stress.

The extramizing solution given by Equation 12c is always unstable while $R = 0$ is stable only for those value of Z less than a critical value of Z, Z'''_c, defined by the bifurcation point. The bifurcation point can be determined exactly from Equation 12c by setting $R = 0$ yielding

$$Z'''_c = \frac{12(12d^4 + d^2 - 3)}{(4d^2-1)^5} \quad (14)$$

Since the right side of Equation 14 is positive for all physically values of $d \geq 1$, from Equation 11 it follows that β must be negative.

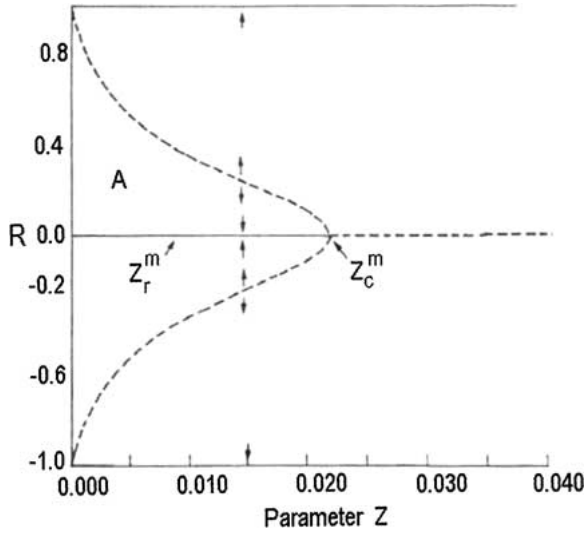

Figure 6 Bifurcation diagram [85] demonstrating the stability against coarsening of two misfitting precipitates. Solid lines depict stable solutions. For large Z, $R = \pm 0.2$ are the only stable solutions. Here $Z_c = 0.22$.

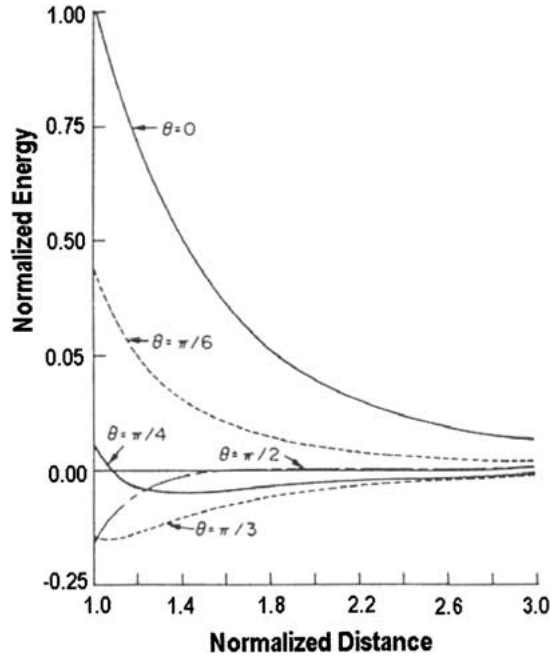

Figure 7 Normalized interaction energy for two misfitting spheres of equal radii subjected to an applied tensile stress [85]. The energy is normalized to and the intercenter distance to the diameter of the precipitate. The parameter $S = 0.9$.

The bifurcation diagram depicted in Fig. 6 is representative of the stability of two misfitting spherical precipitates under the isotropic conditions assumed. The singularity in the behavior of the energy minimum is called a *bifurcation* [92]. The use of well known properties of bifurcations can greatly increase the understanding of the behavior. The bifurcation diagrams examine precipitate stability against coarsening in terms of both the mass distribution between precipitates, R, and the particle orientation with respect to the tensile axis, X. It is also possible to examine the stability of the precipitates with respect to R only, for different levels of applied stress. A small precipitate volume implies a large value of Z for which the only stable solution existing is $R = \pm 1$. Thus the system would be unstable with respect to coarsening. For precipitates of larger size, the associated volume of precipitates increases and Z decreases. Once $Z < Z_c^m$ (the bifurcation point) there are two separate stable solutions, $R = 0$ and $R = \pm 1$.

Fig. 7 examines the interaction energy of two misfitting spherical precipitates subjected to an applied uniaxial tensile stress as a function of intercenter distance and orientation. The total interaction energy is the sum of the interactions owing to the misfit strains, E_{int}^M and applied stress, E_{int}^A. The interaction energy is normalized to $3\psi_{\text{int}}\phi/32\pi$ and the intercenter distance to the diameter of the precipitates when $R = 0$. The sign and magnitude of the interaction depends critically on the orientation of the precipitates with respect to the tensile axis. Energy minima are found for certain orientations intermediate to $\theta = \pi/4$ and $\theta = \pi/3$. Interaction energies as displayed in Fig. 6 are strong functions of the applied stress and precipitate morphology [93].

4. Splitting of γ' particles

Although the classical LSW theory and its subsequent modifications have succesfully explained the ripening behaviour of precipitates in many two phase alloy systems, there are experimental results on the splitting of the precipitate particles which can not be explained by the conventional Ostwald coarsening theories.

A new idea which has been developed [34] on the basis of the so-called "*bifurcation theory*" [85, 94] indicates that, once the precipitate morphology is finely developed, the individual particles hardly coarsen because such a fine microstructure is itself energetically in an extremely stable state as a result of the strong elastic interaction between the particles, i.e. the particles do not need to coarsen or split in order to decrease their energy.

The splitting process occurs in various nickel-base alloys including Ni-Si, Ni-Al-Si and Ni-Al-Ti systems. It was observed that cuboidal γ'-precipitate (Ni_3X) in some Ni-base alloys splits into two or eight small particles (or an group of eight cuboids, i.e., an ogdoad) with a progressive increase in size [30, 95, 41] (see for example Fig. 8a).

The experimental fact of splitting, in spite of increasing the surface energy, seems surprizing. However, this may be understood if it is assumed that the increment in the surface energy is compensated for by the elastic interaction energy between the small particles produced by the splitting. Splitting proceeds by atomic diffusion which requires both time and driving force. Therefore, splitting really occurs at a certain critical size L^{**} which is larger than L^*. It should be pointed out that the splitting phenomenon is observed only when the γ' precipitate particles are sparsely distributed in the γ matrix [30, 33, 41]. It was observed [34] that the γ' split into an ogdoad takes place in the Ni-Al alloy with a large $|\Delta^*|$, where Δ^* is the ratio of the γ–γ' lattice misfit to the surface energy of the γ' particles in the γ matrix ($\Delta^* = \delta/\psi_{\text{int}}$).

Two types of splitting transitions have been observed in cubic materials: the splitting of an isolated cuboid into either two parallel platelike particles (doublet [33] or eight smaller cuboids (octet)) arranged in a cubic geometry with their faces parallel to the {100} cube

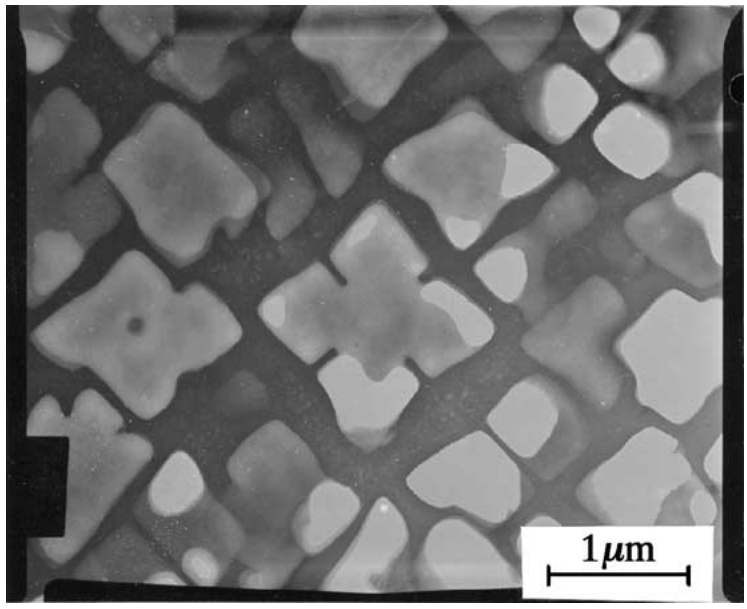

(a)

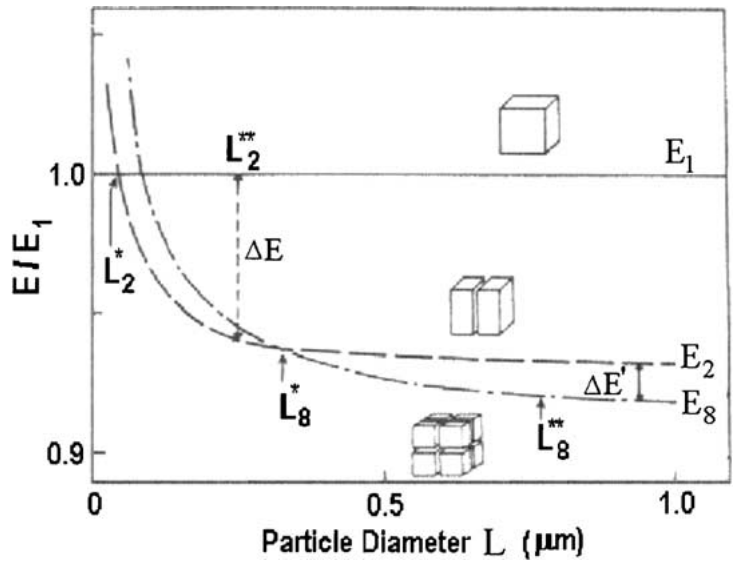

(b)

Figure 8 Effects of elastic strain, surface and elastic interaction energies on the splitting process of γ' particles in nickel-base superalloys. (a) Transmission electron microscopy image of γ' precipitate morphologies in DS 200 + Hf alloy. Note that the single γ' particles are splitting into ogdoads. (b) Comparison between the total energies of a γ' particle in the Ni-Al alloy before and after the split into a doublet or into an ogdoad calculated on the basis of microelasticity theory. E_1, E_2 and E_8 are the total energies in a single state, in a doublet state and in an ogdoad state respectively. The energetically stable shape changes from a single particle to a doublet to an ogdoad with increasing particle size during growth [34].

directions [34]. These transitions have been analyzed in terms of the interfacial and elastic interaction energies between the misfitting particles. Calculations for the Ni-Al system indicate that the system energy is minimized if the morphology of the particles changes progresively from a cube to a doublet to an octet with increasing total particle volume [96, 34]. These calculations are qualitatively consistent with existing experimental observations, although the transition from doublet to octet is not always observed [34].

Doi *et al.* [34] have studied the shape changes of γ' precipitates in nickel-base alloys during continuous cooling by means of transmission electron microscopy. The energetically stable shape of the γ' precipitates was calculated numerically with a computer on the basis of microelasticity theory. In calculating the energies, Doi *et al.* [34] have considered the following three cases: (a) a γ' particle [of volume fraction ϕ and surface area $S(P)$] which is a single inhomogeneous ellipsoid of revolution (with an aspect ratio P) and exist in an infinite γ matrix that is elastically anisotropic, (b) a single γ' particle which splits into two small ellipsoidal γ' particles [of volume $\phi/2$ and surface area $S'(P)$], and (c) a single γ' particle which splits into eight small ellipsoidal γ' particles [of volume $\phi/8$ and surface area $S''(P)$]. E_1, E_2, and E_8, which are the total energies for the three cases (a), (b), and (c) respectively, are expressed by the following Equations [34]:

$$E_1 = \phi E_{\text{incl}}(P) + S(P)\psi_{\text{int}} \tag{15}$$

$$E_2 = 2\frac{\phi}{2} + 2S'(P)\psi_{\text{int}} + E_{\text{int}}^{\alpha\beta}(P) \tag{16}$$

$$E_8 = 8\frac{\phi}{8}E_{\text{incl}}(P) + 8S''(P)\psi_{\text{int}} + E_8(P) \tag{17}$$

where $E_{\text{incl}}(P)$ is the elastic energy of the ellipsoid, ψ_{int} the surface energy density of the ellipsoid, $E_{\text{int}}^{\alpha\beta}(P)$ is the elastic interaction energy between the two ellipsoids produced by the split into a doublet and $E_{8(\text{int})}(P)$ is the elastic interaction energy between the eight ellipsoids produced by the split into an ogdoad. The details of the procedure for calculating the energies have been given elsewhere [33, 41]. Fig. 8b shows the changes in the energy state of γ' precipitates before and after the splits calculated against the diameter L of the single particle before the split for the Ni-Al alloy [34]. When the particle remains small in size, E_1 is the lowest and the particle can stably exist as a single particle. For the particle larger than L_2^*, E_2 becomes the lowest and the doublet is the energetically favorable shape, which suggests the possibility of splitting into a doublet. However, when the particle size becomes larger than the critical size L_8^*, E_8 becomes the lowest and the energetically favourable shape changes from a doublet to an ogdoad. The experimental studies on Ni-Al alloys indicate that the particle size at which the split into a doublet is realized is about 0.25 μm ($=L_2^{**}$) [30, 41]. Doi *et al.* analysis [34] indicates that the size at which the split into an ogdoad is more than 0.5 μm ($=L_8^{**}$) at least. It is considered [34] that the difference between the calculated L_2^* (or L_8^*) and the experimentally obtained L_2^{**} (or L_8^{**}) arises from the kinetics of splitting. An energy difference between E_1 and E_2 at L_2^{**} (i.e. ΔE in Fig. 8b) is regarded as the driving force for splitting a single particle into a doublet. This suggests that the splitting process does not appear until a driving force of ΔE has arisen.

The elastic interaction energy results from the overlap of strain fields which accompany coherent particles. Once the particles lose their coherency, the splitting phenomenon does not take place because of the anhiliation of elastic interaction energy. Further splitting occurs only when the energy diffrence between E_2 and E_8 becomes large enough to split further before the doublet loses coherency.

Doi *et al.* [34] has summarized the theoretical and experimental results for the Ni-Al systems: (a) the γ' precipitate cuboid splits into eight small cuboids during slow cooling but does not split during fast cooling. In the slow cooling case the γ' particles are able to grow larger with decreasing temperature and take the energetically stable state by splitting when their size exceeds a critical value L^{**}. In the fast cooling, however, a large number of small γ' particles are closely aligned along $\langle 100 \rangle$. Such a finely developed microstructure is extremely stable in itself and the particles do not need to grow or split in order to decrease their energy state, (b) when the individual particles grow to a critical size L_8^{**}, the number of particles in the slowly cooled alloys becomes much larger than that in the aged alloys; this results in the diffrence in the density of the unit assemblies formed by the splits.

5. Ostwald ripening

The rate-limiting process in diffusion-controlled coarsening is interparticle diffusion of solute. The chemical-potential gradients that drive this diffusion arise because capillarity causes the chemical potential of solute to be lower in larger particles.

The precipitation of a new phase from a supersaturated solid solution involves three steps (in a continuous precipitation process): (a) Stage 1, *nucleation* of the new phase; (b) Stage 2, *growth* of nuclei using the matrix elements until the matrix reaches its equilibrium concentration of solute; and (c) Stage 3, coarsening of the precipitates through the *Ostwald ripening* process or competitive growth (selective growth).

However, at least two processes occur simultaneously; 1 and 2 or 2 and 3. It is well known that a distribution of immobile particles in a solid matrix tends to lower its interfacial free by transport of matter from the smaller to the larger members of the distribution, thereby diminishing the total particle number but increasing the average particle size. In other words, in stage 3, the surface energy of the precipitate is reduced by coarsening; small ones dissolve and large ones grow at the expense of smaller ones. This coarsening process, known as competitive growth or Ostwald ripening [11], clearly follows kinetics which are in general dependent upon the nature of the particle dispersion, provided that the rate-limiting step is other than the transfer of matter across the particle-matrix interface.

The equilibrium solute concentration $C_m(\rho)$ in the matrix next to the phase boundary to a precipitate of a curvature radius ρ is in general given by the Gibbs-Thomson equation (in general) [97]:

$$C_m(\rho) = C_m(\rho \to \infty)\left[1 + \frac{2\psi_{\text{int}}\Omega}{\rho R_B T}\right] \qquad (18)$$

The Gibbs-Thomson equation is the basic equation which form the beginning of the analysis, where ψ_{int} is the specific interfacial energy of the matrix-precipitate boundary, Ω the molar volume of the precipitate, R_B the Universal gas constant [8.314×10^3 J/(K $\cdot$ kmol)], $C_m(\rho \to \infty)$ the solute concentration in equilibrium with a plane interface, and T the absolute temperature.

Since C_m decreases with ρ, small particles act as solute sources and large particles as sinks. Solute atoms diffuse from the small particles to the large ones.

Ostwald ripening or coarsening, is a phenomenon that occurs in a wide-range of two-phase systems, including liquid-liquid, solid-liquid, and solid-solid mixtures. Much theoretical and experimental work has been done on coarsening driven only by interfacial energy, which governs coarsening in, for example, liquid-liquid systems. In solid-solid systems, however, the morphology of particles is determined in part by the elastic energy that arises from the particle –matrix lattice misfit or an applied stress. The total elastic energy in solid systems can be of the same order as the total interfacial energy, and quantitatively from coarsening driven by interfacial energy alone.

Greenwood [98], Liftshitz and Slyozov [99] and Wagner [97] (i.e., the LSW theory) have analyzed the diffusion nature of Ostwald ripening process, under the assumptions of negligible volume fraction and spherical particles. The process is such that the particle's coarsening is due to the diffusion of the forming precipitate elements through the interface with the matrix.

The coarsening law can be written [97, 99] as

$$\bar{R}^3(t) - \bar{R}^3(0) = Kt \tag{19}$$

where $\bar{R}(t)$ and $\bar{R}(0)$ are the sizes of the particle at time t and 0, respectively and the growth parameter, K is given by

$$K = \frac{8}{9}\frac{\psi_{\text{int}}\Omega^2 DC_e}{R_B T} \tag{20}$$

with ψ_{int} being the surface energy per unit area of the matrix-particle phase boundary (J m^{-2}), Ω the molar volume of the precipitate (m^3 mol^{-1}), D the diffusion coefficient of the constitutive particle element in the matrix (m^{2}s^{-1}), C_e the matrix concentration of such element in equilibrium (mol m^{-3}), R_B the gas constant and T the temperature.

This theory of diffusion-controlled particle coarsening (LSW), can be succesfully applied when the precipitate volume fraction is small, approaching zero [22]. This is not the case for Ni-based superalloys, where the volume fraction is as high as 50% and up to 70 vol% for the ultimate designs of last generation superalloys as CMSX2 or CMSX4 [100]. In addition to this, there exists a consensus on the fact that the elastic coherency stresses induced by the lattice parameter mismatch between the precipitate and matrix, influences the behaviour during the coarsening, and has significant importance when changes in the precipitate morphology appear (41, 101]. The influence of neighbourhood particles over the coarsening behaviour was also analyzed [102, 103]. The extension of the LSW theory to higher volume fractions has been addressed by numerous authors [22–24, 104 –116) and is a field of active interest.

6. Ostwald ripening kinetics of γ' precipitates in nickel-base superalloys

It is well known that the γ'-precipitate morphology is of paramount importance in improving the high temperature strength of nickel-base superalloys. Therefore, one of the important subjects for designing and developing new types of such precipitation-strengthened superalloys is how to control the morphology of γ' particles reduces the creep resistance, because the overaged microstructure allowed deformation to occur by particle by-passing [74, 8, 28, 58]. On the thermal exposure above about $0.6T_m$ (T_m being melting temperature in K), the γ' precipitate ripens (increases in sizes) at a significant rate, facilitating dislocation by-passing. Thus measures that minimize ripening will help retain long-time creep resistance. Therefore, the γ' coarsening can be retarded by changing the Ψ_{int}, C_e and D parameters in the coarsening rate constant K (Equation 20).

6.1. The growth kinetics of γ'-precipitates

In the past there have been much work done on the coarsening kinetics of γ'-precipitate in simple Ni-Al binary alloys and commercial alloys (7, 12, 17, 19, 117–136). In all these studies the mean particle radius $\bar{R}$ of the γ'-precipitates in various Ni-base superalloys was a function of coarsening time, being independent of the applied stress or accumulated strain and the Ostwald ripening particle growth kinetics may be described by the various theories developed for coarsening (see Section 5). Actually, in coarsening phenomenon there are two kinds of theories, namely, the diffusion-controlled growth, and the interface-reaction controlled growth. The general equation for the competitive growth can be written as

$$\bar{R}^n(t) - \bar{R}^n(0) = Kt \tag{21}$$

where the reaction is diffusion controlled rather than interface controlled, the predicted value for n is 3 for coarsening in the matrix, whereas in the interface reaction controlled growth n is 2. However, in the Ni-base superalloys the diffusion-controlled rather than the interface-controlled reactions take place [7]. Therefore, in Ni-base superalloys the growth kinetics of γ'-precipitate can be predicted with the following form of equation:

$$\bar{R}^3(t) = \bar{R}^3(0) + K(\phi)t \tag{22}$$

where ϕ is the volume fraction of precipitates. As mentioned in Section 5, in all the theories of the Ostwald coarsening rate constant $K(\phi)$ would have the form

$$K(\phi) = \frac{A(\phi)D_{\text{eff}}C_e\Psi_{\text{int}}\Omega^2}{R_B T} \tag{23}$$

where D_{eff} is the "effective" diffusion coefficient, Ψ_{int} the particle/matrix interface energy, Ω the molecular volume of the precipitate material, R_B the universal gas constant, T the absolute temperature, and $A(\phi)$ a dimensionless constant.

The value of $A(\phi)$ constant is a dimensionless constant of proportionality whose value is calculated in the Ostwald ripening theories. The magnitude of the dimensionless constant $A(\phi)$ depends on the volume fraction of precipitate; the values yielded by the different theories for some volume fractions ϕ are shown in Table II [19]. The LSW theory was developed for negligible volume fraction. It has proved reasonable so far for these early authors (in the LSW theory) to have ignored volume fraction since experiments show that it has only a small effect, and the theories developed to include the effect of volume fraction (i.e. the MLSW, LSEM and BW theories) manifest a trend, as is evident in Table II.

Equation 22 has been found to be in very good agreement with measurements performed for binary Ni-Al (Ni-rich) [7, 117, 119, 136] and for multicomponent commercial and experimental superalloys [19, 118, 123, 135, 137–141]. Fig. 9 gives an example of good agreement between the experiments [142] and

TABLE II Values of $A(\phi)$ and Ψ_{int} in Equation 23 [Ref. 19]

	$A(\phi)$			
ϕ(%)	LSW	MLSW	LSEM	BW
2	8/9 = 0.89	2.37	1.02	1.16
5	0.89	3.49	1.09	1.44
10	0.89	5.06	1.17	1.75
20	0.89	7.90	1.30	2.19
40	0.89	13.25	1.54	2.98
60	0.89	18.44	1.84	3.69

TABLE III Data for plotting Fig. 10 [19]: all compositions in wt% (1 wt% = 3300 mol m^{-3})

Alloy	Amount of γ' ϕ (vol%)	T (K)	$K(\phi)$ (m^3 s^{-1})	t_o (ks)	Al content of matrix (C)
Ni-5.68 Al	9	773	8.94×10^{-15}	0	4.90
	3	873	1.40×10^{-12}	0	5.24
Ni-6.32 Al	13	923	4.85×10^{-12}	0	5.40
	2	1073	1.52×10^{-9}	0	6.13
Ni-6.71 Al	20	898	2.32×10^{-12}	−4	5.30
	12	1023	1.72×10^{-10}	2.5	5.88
	8	1048	3.89×10^{-10}	−1	6.03
Ni-7 Al	9	1073	1.10×10^{-9}	0	6.13
Ni-8 Al	27	1073	1.06×10^{-9}	−14.5	6.13
Ni- 9 Al	44	1073	1.20×10^{-9}	−25	6.13
Ni-9.9 Al	60	1073	1.30×10^{-9}	−101	6.13
Ni-17.5 Cr-3 Al	23	1023	6.78×10^{-11}	0	1.56
Ni-17.3 Cr-2.7 Al	18	1023	1.14×10^{-11}	0	1.58
Ni-16.9 Cr-3.4 Al	27.5	1023	5.11×10^{-11}	100	1.68
Ni-14.2 Cr-4.9 Al	42	1023	5.11×10^{-11}	100	2.28
IN 738	40–45	1023	4.89×10^{-11}		1.07
		1073	2.0×10^{-10}		1.07
		1123	7.6×10^{-10}		1.07
IN 738		1373	100×10^{-9}	−20	1.42

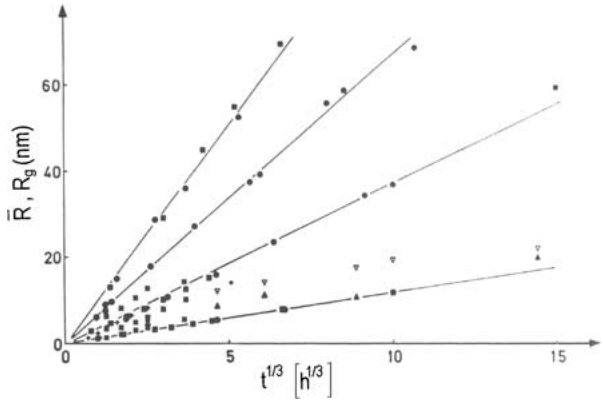

Figure 9 Particle size versus annealing time t [142] for NIMONIC PE 16. T_A annealing temperature; r mean particle radius derived from transmission electron microscopy, R_g radius of gyration derived from small angle neutron scattering. ●: r, $T_A = 949$, 1029, 1079 and 1119 K, ■: r, $T_A = 943$, 1023 and 1113 K, ▲: r, $T_A = 973$ K, △: r_g, $T_A = 973$ K, ∗: r_g, $T_A = 977$, 1021 and 1068 K, +: r_g, $T_A = 1023$ K.

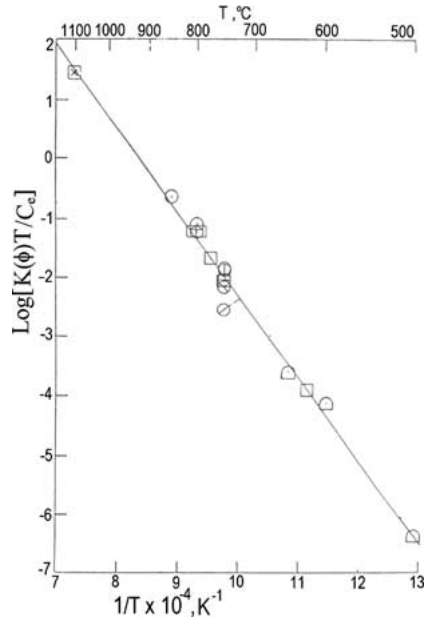

Figure 10 Plot [19] relating growth rate $K(\phi)$ to temperature T and composition C_e in mol m^{-3} (for data see Table III).

Equation 22. Here the mean particle size $\bar{R}$ is plotted against $t^{1/3}$ for NIMONIC PE16.

If Equation 23 is rearranged [19] as

$$\frac{K(\phi)T}{C_e} = \frac{A(\phi)D\Psi_{\text{int}}\Omega^2}{R_B}10^{54} \qquad (24)$$

then $K(\phi)$ has the convenient unit of m^3 s^{-1} when all the quantities are in standard SI units in Equation 24. The right hand side of Equation 24 can reasonably be taken as dependent only on temperature through D, suggesting that $\log[K(\phi)T/C_e]$ be plotted against $(1/T)$. In his review article Mclean [19] used the data in Table III and obtained Fig. 10. As can be seen in this figure the data used in Table III is accordance with Equation 24. From this figure the following equation has been obtained:

$$\frac{K(\phi)T}{C_e} = 6.88 \times 10^{11} \exp\left[-\frac{32520}{T}\right] \qquad (25)$$

Since the left hand side of Equations 24 and 25 are the same the right hand side of these equations must be equal. If the Equation 25 is rearranged as

$$K(\phi) = \frac{2.3 \times 10^{15}}{T} C_e \exp\left[-\frac{32520}{T}\right] \qquad (26)$$

where C_e is expressed in wt% in Equation 26. In Equation 24 the values for parameters are $\Omega = 2.716 \times 10^{-5}$ m^3 mol^{-1} and for Al diffusion in Ni is given by [143]

$$D = 1.87 \times 10^{-4} \exp\left[-\frac{32200}{T}\right] (m^2\ s^{-1}) \qquad (27)$$

Therefore, putting these values into Equation 24 the temperature dependence of Equation 25 has been obtained, which agrees with Fig. 10 within experimental error. Note that in Equations 25 and 26 it is assumed that Al diffusion is to be the coarsening rate controlling factor [19]. It was believed [19] that in Fig. 10

the plot can be used over a wider range of temperature than has been used in the figure. As pointed out by McLean [19], differentiating between a cubic ($\bar{R}^{1/3}$) and square ($\bar{R}^{1/2}$) dependence of the average particle size with time (t) is difficult. McLean has reviewed many of the experimental growth data on γ' in Ni-base superalloys and by converting data obtained at different ageing temperatures to equivalent times at one temperature. He concludes that the cubic rate law fits the experimental data better than the square rate law, confirming again that coarsening in nickel-based superalloys is volume-diffusion controlled.

By replacing $K(\phi)$ in in Equation 22 by its value in Equation 26, the time t under a given combination of T and C_e Mclean [19] has recalculated as equivalent time t_{eq} under some chosen T_{eq} and C_{eq}, thus he has brought all the growth data to a common time base:

$$t_{\text{eq}} = (t - t_o)\frac{T_{\text{eq}}C_e}{TC_{\text{eq}}} \exp\left[32520\left(\frac{1}{T_{\text{eq}}} - \frac{1}{T}\right)\right] \quad (28)$$

T_{eq} and C_{eq} were selected as 1023 K (750°C) and 1 wt%, respectively, and then t_{eq} was calculated for the individual data points ($\bar{a}$, t) presented in Table III. By this means many data points were brought to a common time base in accordance with the theory that produces Equation 22. On plotting as $\bar{a}$ versus $t_{\text{eq}}^{1/3}$ ($\bar{a}$ being half the mean length of the γ' particles edges, and has the unit of m) should yield a straight line if the γ' particles have grown as predicted by the Ostwald ripening theories. These data are plotted in Fig. 11 and do fall close to the straight line. The equation of the graph in Fig. 11 is

$$\bar{a} = 0.329 \times 10^{-9}(t_{\text{eq}})^{1/3} \quad (29)$$

$$\bar{a}^3 = 0.0356 \times 10^{-27} t_{\text{eq}} \quad (30)$$

Of course, Fig. 11 and Equation 29 should be taken as an approximation to the experimental result that is not quite identical with that represented by the plot in Fig. 11.

Mclean [19] has pointed out that Equation 22, with $K(\phi)$ given by Equation 26 can be used to predict growth over service lifetimes in the case of relatively Al-rich nickel-base superalloys.

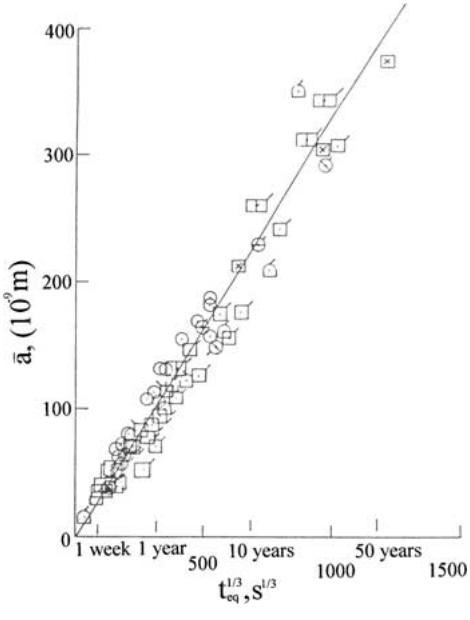

Figure 11 Particle size $\bar{a}$ versus $t_{\text{eq}}^{1/3}$ plot [19].

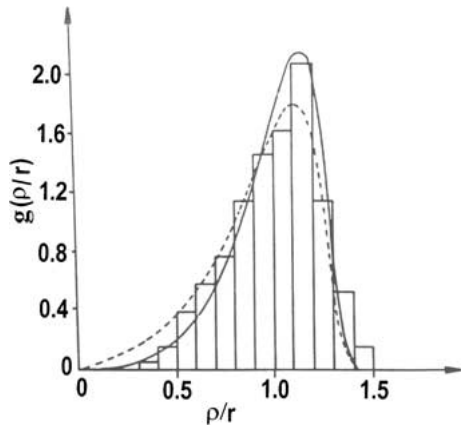

Figure 12 Distribution function g of reduced particle radii (130) ρ/r in Nimonic PE 16. Heat treatment: 21 h at 1119 K, γ'-particle radius: 27 nm; foil thickness: 81 nm, (—): $g_{\text{LSW}}^{(\rho/r)}$, (– – –): $g_{\text{LSW}}^{(\rho \cdot r)}$ adjusted for particles which are visible in the transmission electron microscope though their centres lie outside of the thin foil.

6.2. Particle size distribution of γ'-precipitates

Superalloy specimens heat treated for optimum strength have relatively large particle radii. Therefore the particle dispersion of such specimens is rather stable against further coarsening during the service life. Fig. 12 shows the distribution function g of reduced particle radii $R/\bar{R}$ in Nimonic PE 16, together with the LSW theoretical curve; it is independent of time t. The distribution function for the LSW theory [$g_{\text{LSW}}(\rho)$] is in reasonable agreement with experiments. However, experimental distribution functions are often broader than g_{LSW}. Various investigators have tried to eliminate assumption, i.e. to treat the more realistic case of finite and even of large volume fractions. Finite values of volume fraction ϕ lead to a broadening of the distribution function of particle radii(see Section 5).

Hoopgood *et al.* [130] have investigated coarsening kinetics of single crystal SRR99 superalloy. They have

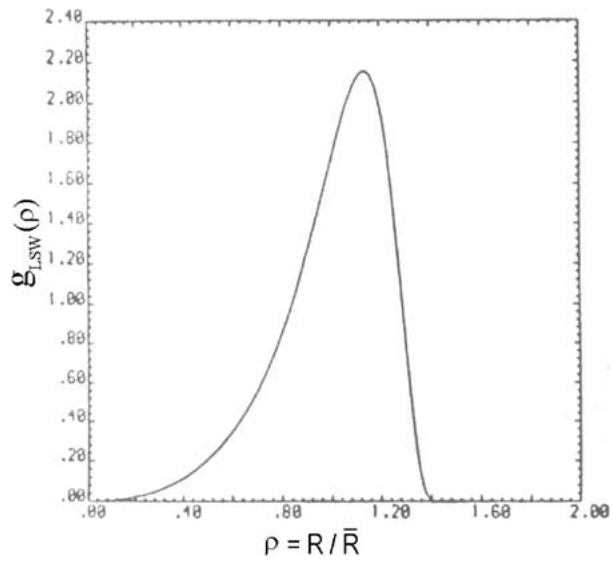

Figure 13 The relative particle size distribution predicted by the LSW theory. The quantity ρ is the linear particle size divided by the mean size ($R/\bar{R}$) and $\rho = 1.5\ \bar{R}$ is the maximum value allowed.

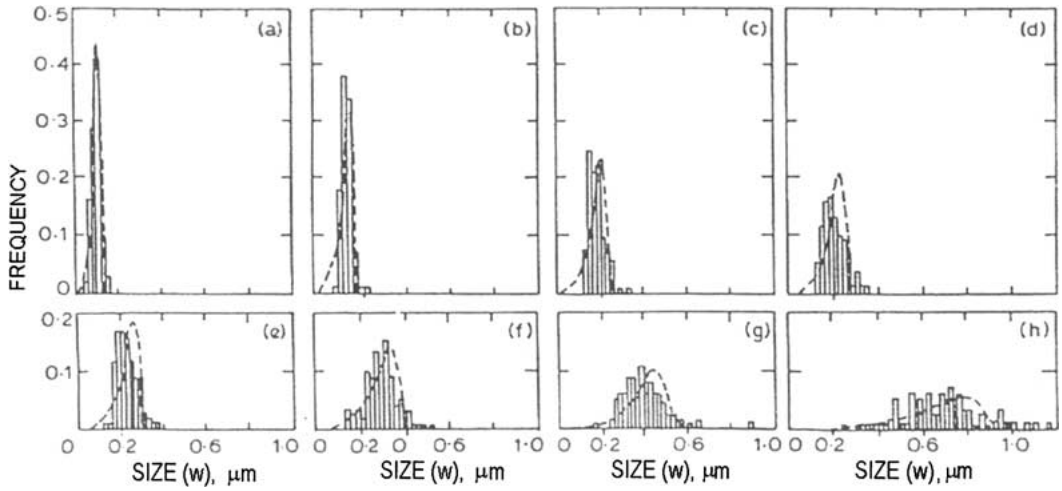

Figure 14 Size distribution [130] of γ'-precipitate produced by aging at 1100°C for various times in single crystal SRR99 superalloy: distributions predicted by LSW theory for mean precipitate size equal to experimental value are shown as dashed lines. (a) Unaged; (b) 0.167 h; (c) 0.5 h; (d) 1 h; (e) 1.5 h; (f) 4 h; (g) 11 h; (h) 72 h.

measured the precipitate size from the microstructures produced by aging at 1100, 1000, 900, and 800°C. The experimentally determined values for the mean size and theoretical distributions predicted by the LSW theory (Fig. 13) for precipitate coarsening are shown in Fig. 14. As this figure shows there is good correspondence between the shapes of the experimental distributions and those predicted by the LSW theory at each temperature after short aging times. After long aging times the experimental distributions become broader than the theoretical distributions and in particular some precipitates have sizes greater than 1.5 of the mean, which is not permitted by the LSW theory. A broadening of the right-hand edge of the size distribution function has been predicted by those theories of Ostwald ripening which include modifications to take account of precipitate volume fraction.

6.3. Application of Ostwald ripening theory to the γ'-precipitate growth

Molen *et al.* [134] have investigated the particle coarsening kinetics of γ'-precipitates in Udimet 700 at different aging temperatures. For this purpose the following equation was used:

$$[\bar{R}^3(t) - \bar{R}^3(0)]^{1/3} = k(\phi)t^{1/3} \qquad (31)$$

The coarsening characteristics of γ' has been investigated extensively in the Ni-Al system [i.e. 7, 11, 119, 144]. The particle growth data for the Ni-base superalloys containing 6 wt% Al showed that the coarsening behaviour of γ' was in good agreement with the LSW theory. The LSW theory has also been successful in describing the coarsening characteristics of Ni-Ti [11, 119] and Ni-Si [11, 145] alloys. However, in Ni-Si alloy after 16 hours of ageing at 775°C, a departure from the $t^{1/3}$ kinetics was observed. This deviation from linearity was associated with the loss of coherency of the γ' particles.

Following Ardell [7, 119], for cuboidal particles $\bar{R}$ was replaced by $\bar{a}/2$ where $\bar{a}$ is the average length of a cube edge, i.e.

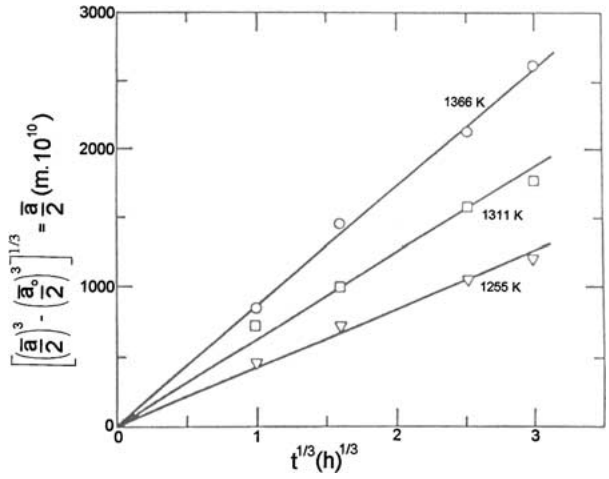

Figure 15 The $t^{1/3}$ dependence of average particle size ($\bar{a}/2$ versus $t^{1/3}$) [134].

$$\left[\left(\frac{\bar{a}}{2}\right)^3 - \left(\frac{\bar{a}_o}{2}\right)^3\right]^{1/3} = k(\phi)t^{1/3} \qquad (32)$$

The particle data were therefore presented as a plot of $[(\bar{a}/2)^3 - (\bar{a}_o/2)^3]^{1/3}$ versus $t^{1/3}$ in Fig. 15. The data are consistent with a linear relationship and thus with the Ostwald ripening theories in which large particles grow at the expense of small ones (selective or competitive growth) by a diffusion-controlled mechanism.

The slope of each curve in Fig. 15 is a temperature dependent rate constant $k(\phi)$ which is given in Equation 33, which was used by Molen and co-workers [134], and is given below:

$$k(\phi) = \left[\frac{8}{9}\frac{\psi_{\text{int}}\Omega^2 DC_e}{R_B T}\right]^{1/3} = K^{1/3}(\phi) \qquad (33)$$

The Equation 33 can be rearranged to give:

$$\text{Ln}\left[k^3(\phi)\left(\frac{T}{C_e}\right)\right] = \text{Constant} - \frac{Q}{R_B T} \qquad (34)$$

Thus plots of Ln $[k^3(\phi)(T/C_e)]$ versus $(1/T)$ yield Q from the slope and D_o from the intercept. The activation

TABLE IV Data for the determination of the activation energy Q and the constant A of Equation 34 [134]

Temperature (T) (K)	$k^3(\phi)$, (m h$^{-1/3}$ × 10^{10})	C_e (at.%)	$k^3(\phi)T/C_e$ (m^3 K h^{-1} × 10^{30})
1144	156	6.60	6.61
1172	202	6.76	14.40
1200	286	7.35	37.90
1227	328	7.48	57.60
1255	420	8.05	115.5
1283	503	8.92	183.0
1311	625	9.78	328.0
1339	744	10.31	532.0
1366	864	11.18	785.0

energy (Q) for coarsening for γ'-precipitates in Udimet 700 was calculated from the plot of Ln $[k^3(\phi)(T/C_e)]$ versus $(1/T)$ given in Fig. 16 (the data [134] for the plot is given in Table IV). The values of Ln $[k^3(\phi)(T/C_e)]$ vary linearly with $(1/T)$. The values of $k(\phi)$ for 1255 K, 1311 K, and 1366 K were obtained by measuring the slope of the particle coarsening curves in Fig. 15. From Fig. 16 the activation energy for Udimet 700 was measured to be 269.6 kJ/mole (64.5 kcal/mol). Despite the complex nature of this alloy, the activation energy correlates well with that for diffusion of Al or Ti in Ni (269.2 and 267.9 kJ/mole, respectively) [7, 121] and to coarsening of γ' precipitates in simple binary Ni-Al alloy [269.2 kJ/mole].

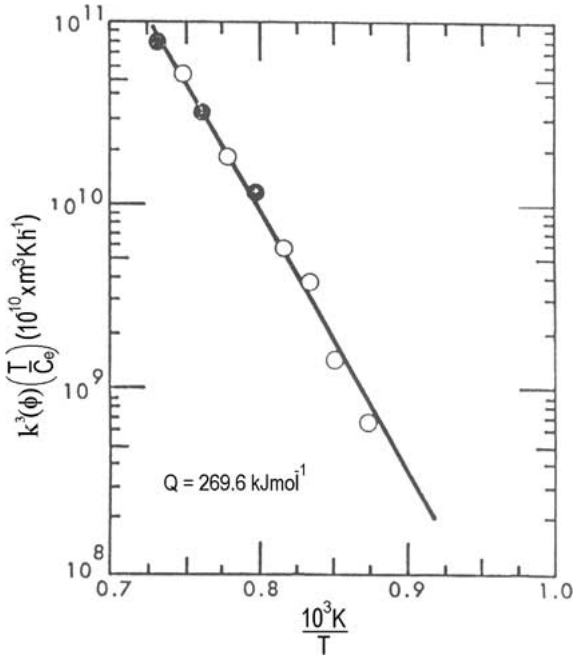

Figure 16 Determination of the activation energy (Q) for coarsening [134].

For Udimet 700 the rate of coarsening can be given by, as in Equation 26:

$$\left[\left(\frac{\bar{a}}{2}\right)^3 - \left(\frac{\bar{a}_o}{2}\right)^3\right]^{1/3} = A^{1/3}t^{1/3}\left(\frac{C_e}{T}\right)^{1/3} \times \exp\left[-\frac{64500}{2.303R_BT}\right] \quad (35)$$

where $A = 12.7 \times 10^{-4}$ (m K/h$^{1/3}$) for concentration C_e of (Al + Ti) in at. pct. solute. This information (Equation 35) is sufficient for evaluating the parameters in the coarsening equation.

A series of particle size versus time plots using Equation 34 are presented [134] in Fig. 17 for temperatures from 1033 to 1366 K. Such a chart (Fig. 17) can be used to predict the effect of thermal exposure upon the volume fraction and particle size of the γ' precipitate or as a guide to heat treatment. For example, one could produce a distribution of γ' particles 18×10^{-8} m (1800 Å) (on a cube edge ($\bar{a}/2 = 900$ Å $= 9 \times 10^{-8}$ m) where the amount of γ' varied from 14 vol% (1.2 h at 1366 K) to 38 vol% (65 h at 1172 K).

6.4. Evaluation of ψ_{int}, D, C_e, and Q parameters

It was shown [11, 146, 147] that studies of particle coarsening can be exploited to obtain reliable numerical values of several parameters commonly encountered in solid state precititation kinetics. The parameters of interest are: (a) the precipitate-matrix interfacial

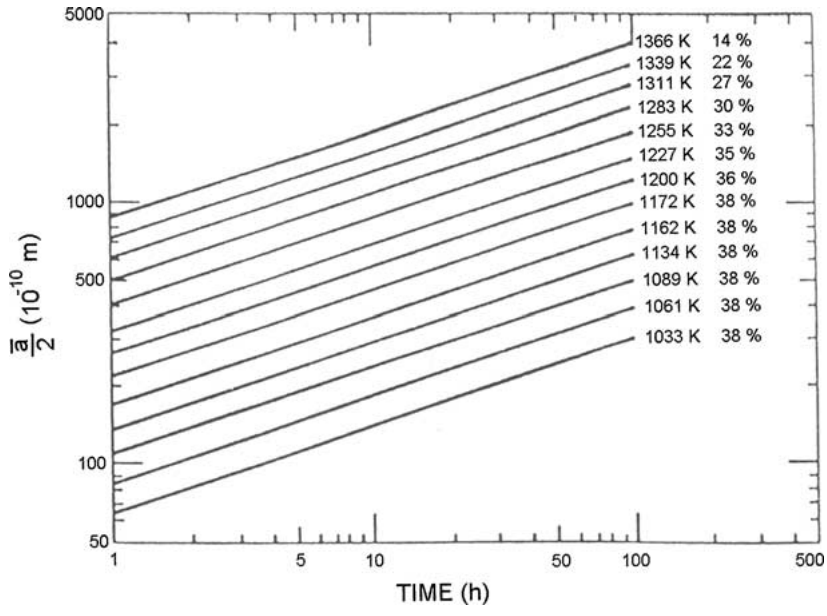

Figure 17 Average γ' particle size ($\bar{a}/2$) versus time for temperatures [134] from 1033 to 1366 K (volume fraction of γ' from 38 to 14%).

free energy (Ψ_{int}), with the understanding that Ψ_{int} may be a function of the orientation of the interest; (b) the "effective" diffusivity of the component species of the particle, D_{eff}, which generally differs from the solute diffusivity because of certain physical constraints that may act upon a particle growing in a solid matrix [148]; and (c) the solubility in equilibrium with a particle of infinite size, C_e. Specifically, experimental values of Ψ_{int} and D_{eff} can be determined directly by the methods described by Ardell. As desribed below, the values of D_{eff} obtained for Ni-Al and Ni-Ti alloys [11] agreed fairly well with the extrapolated values obtained independently from standard high temperature diffusion experiments [143].

In order to extract values of these parameters from coarsening data it is necessary to measure independently both the average particle size and the average concentration (C) of solute in the matrix as a function of ageing times.

In the LSW theory the average particle size as a function of time can be described as (see Section 5, Equation 19):

$$\bar{R}^3(t) = \bar{R}^3(0) + Kt \tag{19}$$

and K is a coarsening rate constant given by

$$K = \frac{8}{9}\frac{\psi_{int}\Omega^2 D C_e}{R_B T} \tag{20}$$

The average concentration, C, of solute in the matrix is related to the average particle radius $\bar{R}$, by the Gibbs-Thomson equation

$$C - C_e = \frac{2\Psi_{int} C_e \Omega}{\bar{R} R_B T} \tag{36}$$

The following is the Ardell's treatment [146, 149] about the variation of average solute concentration (C) of the matrix: Letting $\Delta = C - C_e$, the relationship between Δ and t is obtained simply by rewriting Equation 36 for $\bar{R}$ and substituting the result into Equation 19, whereby we obtain

$$\frac{1}{\Delta^3} - \frac{1}{\Delta_o^3} = \chi t \tag{37a}$$

where

$$\Delta_o = C_o - C_e \tag{37b}$$

$$\chi = \frac{D(R_B T)^2}{9\psi_{int}^2 C_e^2 \Omega} \tag{38}$$

At long aging times the asymptotic behavior $1/\Delta_o$ is negligible compared with $1/\Delta^3$. So that Equation 37a reduces [146, 149] to

$$\frac{1}{\Delta^3} \cong \chi t$$

$$C - C_e \cong (\chi t)^{-1/3} \tag{39}$$

C_e is the equilibrium concentration of solute in the matrix. The parameter C_e is a true thermodynamic equilibrium solubility because it defines the solute content of the matrix in equilibrium with a particle of infinite size. This is the state of the system that will exist at $t = \infty$. To obtain C_e at a given temperature, it is necessary only to plot C versus $t^{-1/3}$ and extrapolate the curve to $t^{-1/3} = 0$.

According to the theory of diffusion controlled coarsening, the average concentration of solute C, in the matrix phase varies with time t according to Equation 39. In other words, Equation 36 describes the asymptotic variation of the solute content (C) of the matrix with ageing time.

Equation 39 is an approximation [146] which is not accurate at the beginning of the coarsening process. However, the error involved in Equation 39 over whole range of aging times is generally small. Equation 39 is particularly convenient to use for the purpose of evaluating C_e and χ.

The parameters Ψ_{int} and D are readily evaluated from the experimental values of $\chi^{-1/3}$ and $k^{1/3}(\phi)$ (the slope of the plot in Fig. 15) according to the following equation [119, 146]:

$$\Psi_{int} = \frac{\left[\dfrac{k(\phi)}{\chi}\right]^{1/3} R_B T}{2C_e\Omega} \tag{40}$$

$$D = \frac{9}{4}\frac{[k^2(\phi)\chi]^{1/3}}{\Omega} \tag{41}$$

In summary, the values of Ψ_{int} and D can be obtained if the variations of the mean particle radius $\bar{R}$ and the average concentration of the solute C in the matrix as a function of time can be measured independently using the experimentally determined values of K and χ.

It is useful to illustrate the evaluation of Ψ_{int}, D and Q and C_e parameters because these parameters are very important in the study of Ostwald ripening. Ardell [121] has studied the growth kinetics of the γ' precipitate in a Ni-8.74 wt% Ti alloy. The variation of the titanium content of the nickel-rich matrix is shown as a function of aging time at 965 K, 866 K, and 796 K in Fig. 18, which is consistent (apart from the concentration units) with the theoretical equation (Equation 39). The values of W_{Ti} (in wt%) approaches the predicted linear dependence on $t^{-1/3}$ after aging times that are clearly temperature dependent: $\cong$20 min. at 965 K; $\cong$1 hr at 866 and $\cong$16 h at 796 K. It is emphasized that these aging times do not necessarily represent the times at which coarsening actually commences, because Equation 39 is an approximation which is not accurate at the beginning of the coarsening process. Let us now evaluate the C_e and χ using Fig. 18 (or Equation 39). The data in Fig. 18 indicates the linear regions, which were least-squares analysed to obtain values of the intercepts (C_e or W_e) and slopes ($\chi^{-1/3}$) of the curves. The values of these parameters are given [121] in Table V.

According to Equation 39 the activation energy for the coarsening process can be obtained by plotting

TABLE V Results [121] of the least-squares analysis of the data in Fig. 19

T (K)	$\chi^{-1/3}$ (mole s$^{1/3}$ m^{-3} $\times 10^{24}$)	W_e (or C_e) $\times 10^2$
796	4.050×10^{-1}	6.633
866	1.235×10^{-1}	7.268
965	3.455×10^{-2}	8.123

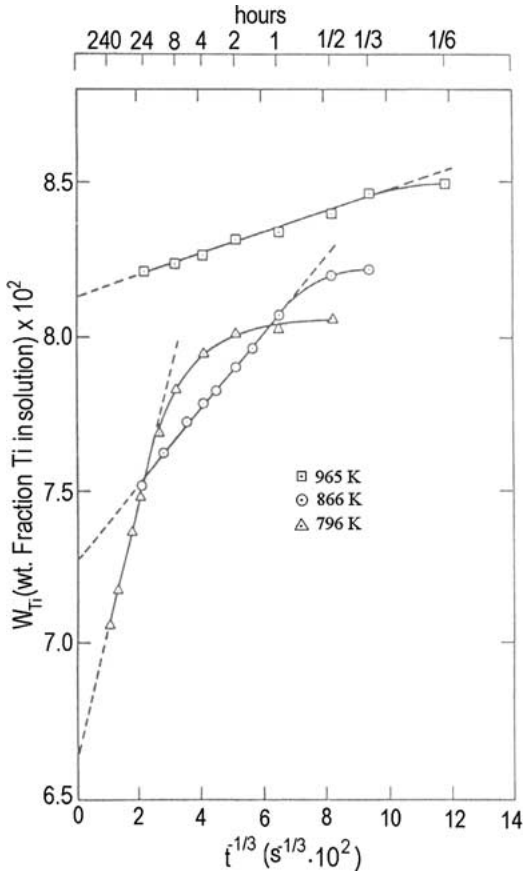

Figure 18 The variation [146] of Ti content in Ni-rich matrix during growth of the γ' precipitate, plotted as weight fraction Ti versus $t^{-1/3}$.

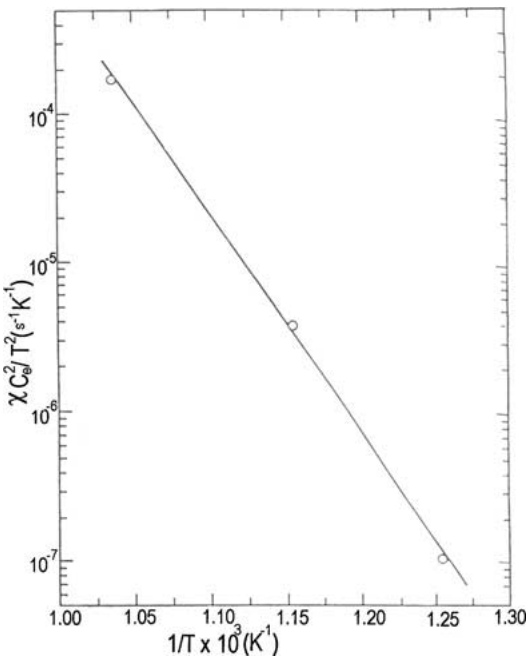

Figure 19 Plot [121] of the rate constant χ multiplied by the temperature dependent factor C_e^2/T^2 versus the reciprocal of the absolute temperature.

$\text{Log}(\chi W_e^2/T^2)$ versus $1/T$. A plot of this type is shown in Fig. 19. The resulting activation energy is 282.2 kJ/mole, which is in fair agreement with the reported value of 256.7 kJ/mole for the diffusion of Ti in very dilute Ni-Ti alloy [143].

The parameters Ψ_{int} and D are evaluated from the experimental values of $\chi^{-1/3}$ and $k^{1/3}(\phi)$ according to

TABLE VI Estimated values of Ψ_{int} and D from the application of coarsening theory to 965 K data [121]

Ψ_{int} (J m^{-2})	D (m^2 s^{-1})	D (m^2 s^{-1})[a]
0.0213	1.51×10^{-18}	1.08×10^{-18}

[a]Calculated from the equation $D = 0.86 \exp[-61400/(R_B T)]$ given by Swalin and Martin [143, 150].

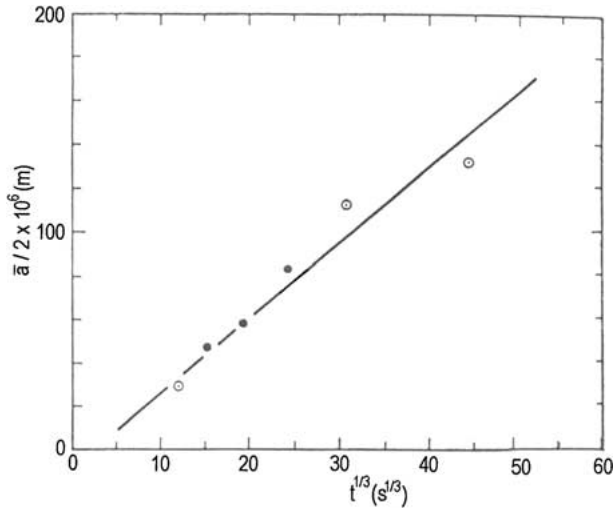

Figure 20 Plot [121] of $\bar{a}/2\gamma'$ particle edge length versus $t^{1/3}$ for a Ni-8.74 wt% Ti alloy aged at 692°C.

the Equations 40 and 41. K is determined from the slope of the plot in Fig. 20. Substitution of the values of the parameters in Equations 40 and 41 for aging at 965 K gives:

$$k^{1/3}(\phi) = 3.47 \times 10^{-16} \text{ m s}^{-1/3}$$
$$\chi^{-1/3} = 6.42 \times 10^{-21} \text{ mole s}^{1/3} \text{ m}^{-3}$$
$$\Omega = 27.83 \times 10^{-24} \text{ m}^3 \text{ mol}^{-1}$$

The values of Ψ_{int} and D determined from the above results are shown in Table VI. The value for the diffusivity (D^*) of Ti in dilute Ni-Ti alloys, obtained by extrapolating the data from ref. 56 to 965 K, is also shown [121] in Table VI.

7. Concluding remarks

The most widely applicable process for nickel-base superalloys for the decomposition into a two-phase mixture is that of nucleation, growth and coarsening [149]. The overall reduction of precipitate surface area is the driving force behind the growth of particles larger than some critical size at the expense of smaller ones. This process is known as both coarsening and Ostwald ripening. In nickel-based superalloys strengthened by the γ' phase, based on Ni_3Al, the kinetics of coarsening of γ' particles have attracted considerable attension over the past four decades. Investigations have been made on "model" alloys such as Ni-Al [7, 32, 119, 151], Ni-Al-Cr [22, 32, 122, 151], Ni-Al-Co [152], Ni-Al-Mo-Ta [153] and Ni-Al-Mo-W [153], as well as in certain complex industrial alloy systems [25, 28, 134, 143, 154, 155].

Coarsening experiments performed upon nickel-base superalloys are generally interpreted as showing diffusion-controlled growth. However, scatter in experimental data generally makes it impossible to distinguish diffusion-controlled from interface-controlled growth, since data often fit $t^{1/3}$ and $t^{1/2}$ approximately equally well. As mentioned previous section, the study performed by McLean [19], however, showed that long-term coarsening behaviour really does follow diffusion-controlled growth behaviour (i.e. $t^{1/3}$) in several binary and ternary alloys, thus demonstrating the existence of diffusion-controlled growth mechanism of γ' precipitates in Ni-base superalloys. γ' coarsening by diffusion control has been found to commence at a very early stage in the ageing process. An investigation [151] of γ' precipitates in Ni-Al and Ni-Al-Cr alloys has shown that the experimentally determined particle size distributions of γ' had a good agreement with those predicted by the BW theory. However, as McLean [19] pointed out in his review study on the nickel-based superalloys, γ' particle-size distributions (PSDs) are better fitted by the encounter-modified LSW model (i.e. the LSEM theory).

Irrespective of the rate controlling mechanism for Ostwald ripening, it is the reduction in total interfacial energy Ψ_{int} which drives the process. It is, therefore, appealing to say that the difference in coarsening rates (K) are due to a reduction in interfacial energy due to a reduction in the lattice mismatch between matrix and particles [156]. Some previous work [32, 145] reports that the particle size distribution (PSDs) broadens with an increase in lattice mismatch. However, in contrary to this, a study [151] on the Ni-Al and Ni-Al-Cr systems has shown that an increase in lattice mismatch did not affect the PSD.

7.1. Ostwald ripening kinetics of γ' precipitates

Activation energies for coarsening of γ' precipitate particles and for diffusion, and interfacial energies between γ' particles and γ-matrix can be determined by proper manipulation of data from coarsening studies [11, 22, 146]. Namely, using particle coarsening theory, specifically the pioneering works described by Ardell, these parameters are obtained if the concentration changes during coarsening can be measured precisely.

According to the LSW theory for particle growth from an initially supersaturated solid solution, there are two stages of growth for the average particle size. Initially the precipitates grow by diffusion of solute directly from the local matrix. The growth rate of the average particle size, $\bar{R}(t)$, can be expressed as

$$\bar{R}^2(t) = 2D\Delta_o t \tag{42}$$

where D is the solute diffusion coefficient in the matrix, t is the time and the initial supersaturation is given

$$\Delta_o = C_o - C_e \tag{37b}$$

where C_o is the initial concentration, and C_e the concentration of solute in the matrix at equilibrium with an infinitely large second phase particle. In the second stage the particles start competing for solute and the larger particles start competing for solute and the larger particles grow at the expense of those smaller ones. This process is called Ostwald ripening or coarsening. The kinetics of this process are described by Equation 19.

As coarsening proceeds the degree of supersaturation of the matrix with solute, $\Delta(t)$, decreases as [157]

$$\Delta(t) = C(t) - C_e \cong [\chi(t - t_o)]^{-1/3} \tag{43}$$

where $C(t)$ is the average concentration of solute in the matrix at time t, and χ is given by

$$\chi = \frac{D(R_B T)^2}{9\psi_{\text{int}}^2 C_e^2 \Omega} \tag{38}$$

Although the LSW theory assumes a fixed volume fraction of precipitate in its description of the asymptotic coarsening case, in reality, for a constant amount of solute the volume fraction of the second phase, ϕ, must increase as the matrix concentration of solute decreases. Following Ardell [11], who assumes an overall conservation of solute, the relationship of the volume fraction to the weight fraction of solute in the matrix, w, is

$$\phi = \frac{w_0 - w}{w_{\gamma'} - w} \tag{44}$$

where w_0 is the total weight fraction of solute in the alloy and $w_{\gamma'}$ is the weight fraction of solute in the precipitate phase.

The equilibrium value of the volume fraction, ϕ_c, for the totally completed decomposition reaction is obtained from this formula by setting w equal to the equilibrium value w_e obtained from the phase diagram at the appropriate composition. Taken together, Equations 38 and 44 yields an expression for the time dependence of the volume fraction [157]

$$\phi(t) = \phi_c - [\chi * (t - t_o)]^{-1/3} \tag{45}$$

where

$$\chi* = \left(\frac{w' - w_e}{1 - \phi_e}\right)^3 \chi \tag{46}$$

In Equations 20 and 38 the only unknown quantities are the diffusion coefficient, D, and the precipitate-matrix interfacial energy, ψ_{int}. It is convenient to define two experimentally determined variables [157]:

$$\alpha = \left[\frac{k(\phi)}{\chi}\right]^{1/3} \tag{47}$$

and

$$\beta = [k^2(\phi)\chi]^{1/3} \tag{48}$$

Within the derivation of the LSW formula it is assumed that the precipitate is entirely made up of solute. This asumption allows the use of the following approximation [157]:

$$C_p - C_e \cong \frac{1}{\Omega_m} \tag{49}$$

where C_p is the solute concentration in the precipitate. Equation 49 is valid as long as $C_p \gg C_e$ [158]. Since $C_p = 0.236$ [159, 160], and a representative value of

TABLE VII Coarsening rate results for different results and crystallographic direction in Ni-12.5 at.% Al alloy [157]

T (K)	$[hkl]$	$K(\phi)$ ($m^3 \cdot h^{-1} \times 10^{30}$)
823	110	20.9
873	110	31.4
898	110	85.2
898	100	98.0
923	110	113.0
948	110	613.0
948	100	215.0
973	110	638.0
973	100	271.0

TABLE VIII Results of integrated intensity analysis for Ni-12.5 at.% [157]

T (K)	χ ($m^9\ s^{-1}\ mol^{-3} \times 10^{18}$)
773	298.0
873	208.0
923	1660.0
973	39300.0

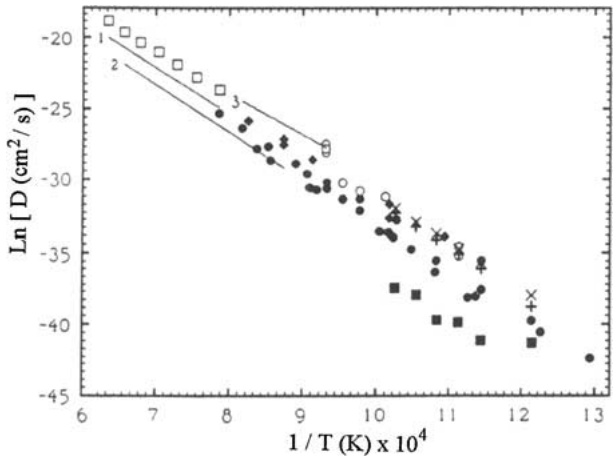

Figure 21 Comparison of diffusion coefficient results for different literature values [157]. Key: Line "1": best fit from [143], Line "2": best fit from [163], Line "3": best fit from [164], □: Al in polycrystalline Ni [165] ○: Al in polycrystalline Ni [7, 32, 119], ■: Ref. 157, ●: Ni-self diffusion in single crystals [166–168], and volume constrained calculations of Li and Oriani using both, ×: polycrystalline values [143, 164], +: Single crystal values [166, 169].

C_e is 0.11 [161], one can see that the approximation is invalid. Within this change, Marsh and Chen [157] has developed the following expression for the coarsening rate:

$$K(\phi) = \frac{8\Omega D \psi_{\text{int}}}{9 R_B T}\left(\frac{C_e}{C_p - C_e}\right) \tag{50}$$

Expressions for both D and ψ_{int} in terms of known quantities are given by [157]

$$\psi_{\text{int}} = \left[\frac{R_B T}{2C_e}\left(\frac{C_p - C_e}{\Omega^2}\right)^{1/3}\right]\alpha \tag{51}$$

$$D = \frac{9}{4}\left[\frac{(C_p - C_e)^2}{\Omega}\right]^{1/3}\beta \tag{52}$$

Applying Equations [50–52], Marsh and Chen [157] has studied the kinetics of the particle-growth of the γ' particles during the precipitation reaction of a supersaturated solid solution single crystal of Ni-12.5 at.% Al alloy at moderately high temperatures using an *in situ* X-ray diffraction technique. The corsening rate, $K(\phi)$, determined at different crystallographic directions for different temperatures, is shown in Table VII [157], which indicates the $t^{-1/3}$ dependence. From these plots the rate constant, χ, is obtained and listed in Table VIII for four temperatures.

One of the assumptions inherent in the LSW theory is that of a fluid matrix which is clearly not the case for a solid solution. Li and Oriani [162] have employed a volume constraint criterion for the solid state coarsening of coherent precipitates to arrive at an expression for the "effective" diffusivity of the solute in the matrix

$$D_{\text{eff}} = \frac{X_{\text{Ni}} D_{\text{Al}} + D_{\text{Al}} D_{\text{Ni}}(1 + X_{\text{Al}}/X_{\text{Ni}})}{X_{\text{Ni}} D_{\text{Ni}} + X_{\text{Al}} D_{\text{Al}}} \tag{53}$$

where X_{Ni} and X_{Al} represent the mole fraction of the components in the matrix. For diffusion values of Al and Ni in polycrystalline Ni samples the values of Swalin and Martin [143] and Hofman *et al.* [163], respectively, are used. For the difusion values of Al and Ni in Ni single crystals the values of Gust *et al.* [169] and Wazzan [167], respectively, are used. These calculated values of D_{eff} along with other representative values from the literature are shown in Fig. 21. As can be seen, the volume constraint correction appears to have little effect and the values obtained are comparable to experimental values.

As seen in Fig. 21 the results of this study show a similar activation energy as well as a consistently lower D_{o} or entropy factor. The activation energy obtained by a least squares fitting of the data neglecting the 823 K data point is 262.5 ± 18.4 kJ mole^{-1}. This compares well with an average value of 266.3 kJ mole^{-1} obtained from other experimental data displayed in Fig. 21 with a range of 234.5–303.5 kJ mol^{-1}.

The values for D and ψ_{int} found for a single crystal of Ni-12.5% Al alloy by using Equations 51 and 52 as well as the experimental results in Tables VII and VIII are shown in Tables IX and X along the values obtained by other researchers. The molar volume, Ω, of the precipitate is based on a stoichiometric "molecule" of Ni_3Al. Ω is calculated using $\Omega = N_A a^3$, where N_A is Avogadro's number and a is the lattice parameter of the

TABLE IX Calculated diffusion values [157] for Ni-12.5 at.% using the volume constraint relation of Li and Oriani [162] after the method of Ardell [119] usin: (a) polycrystalline [143, 163], and (b) single crystal [166, 169] measured diffusion coefficients for the constituent elements [157]

T (K)	Ln(D_{a})	Ln(D_{b})
823	−37.93	−38.80
873	−35.73	−36.16
898	−34.73	−35.14
923	−33.78	−34.17
948	−32.88	−33.26
973	−32.02	−32.29

TABLE X Experimentally determined values [157] of interfacial energy ψ_{int} (mJ m^{-2}) for Ni-12.5 at.%

T (K)	$\psi_{(int)a}$	$\psi_{(int)b}$	$\psi_{(int)c}$	$\psi_{(int)d}$	$\psi_{(int)e}$
823	16.9	–	–	–	–
848	–	22.0	–	–	–
873	21.7	–	–	–	–
898	–	–	14.4	–	–
923	16.6	–	–	–	–
943	–	–	–	17.4	–
953				16.6	
963				19.6	
968				24.3	
973	10.3				
988			14.2		
1073					6.2, 8.9, 11.9, 8.3

Note that the data in Table X were taken from the following references: a = Ni-12.5% Al [157]; b = Ni-15.4 at.% Al [131]; c = Ni-6.35 and 6.71 wt.% Al averaged [119]; d = Ni-12.29% Al [170]; e = Ni-7.0, 8.0, 9.0, 9.9 wt.% [32], respectively.

unit cell. Using $a = 3.567 \times 10^{-10}$ m [160]. Ω is found to be 27.34×10^{-6} m^3 mol^{-1}.

Changes in composition would alter the coarsening rate, $K(\phi)$ by directly affecting Ψ_{int}, C_e and D. For example, alloying elements Co and Mo are believed to retard growth of the γ' precipitate particles [45]. Chromium has been found to reduce the solubility of Al in the γ phase, thus reducing coarsening rates [171]. However, this finding has been contradicted by others [172]. Also decreasing the Ti : Al ratio decreases the γ' coarsening rate [43]. On the other hand, rhenium reduces coarsening rates in Ni-base superalloys [173], at least in short-term experiments. In this study, it is suggested that coarsening of γ' is controlled by diffusion of Re away from the particles.

Kim *et al.* [21] have investigated the growth kinetics of the γ' precipitate in two "model" nickel-base cast superalloys with higher strength and longer creep rupture lives than advanced conventionally cast Ni-base superalloy Mar-M247. The alloys studied have the following main compositions: Alloy 1: Ni-4.35% Al-10.4% Cr-8.02% W-1.75% Mo-1% Ti; Alloy 2: Ni-4.52% Al-8.48% Cr-9.68% W-1.76% Mo-0.95% Ti. Fig. 22 shows that the γ' in these alloys obeys the $t^{1/3}$ law, suggesting that the coarsening of γ' in these complex, high volume fraction superalloys also follows the standard $t^{1/3}$ kinetics of diffusion-controlled particle growth. Similar observations of the cubic growth kinetics of γ' have also been made in a number of nickel-base superalloys [26–28].The slop of each line in Fig. 22 is a temperature dependent rate constant $k(\phi)$ [or $K^{1/3}(\phi)$] which can be used to determine the activation energy Q. It is necessary to plot $\ln[k^3(\phi)T]$ versus T^{-1} as in Fig. 23 to obtain Q values. This yields activation energies of 272 and 277 kJ mol^{-1} for Alloy 1 and Alloy 2. Despite the complexity of these alloys, the activation energies correlate well to that for the volume diffusion of both aluminum and titanium in nickel (270 and 257 kJ mol^{-1} [143], respectively), to the coarsening of γ' in binary Ni-Al and Ni-Ti alloys (270 and 257 kJ mol^{-1} [121], respectively), and to the coarsening of γ' in binary Ni-Al and Ni-Ti alloys (270 [7] and 282 kJ mol^{-1} [121], respectively), and to the coarsening of γ' in Udimet 700 (270 kJ mol^{-1}) [21]. These results indicate that the growth of γ' in the alloys is controlled mainly by the volume diffusion of aluminum or titanium in the matrix.

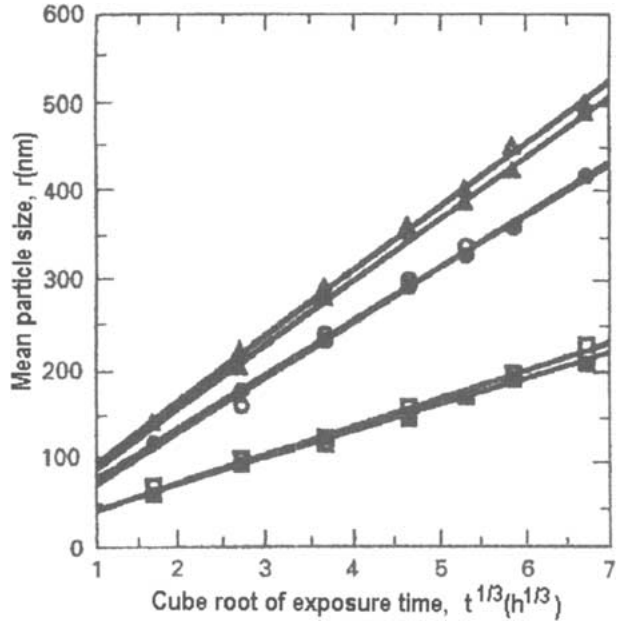

Figure 22 Variation in mean particle size of γ'-precipitates with ageing time at various ageing temperatures [21]. Key: □: 1143 K, alloy 1; ○: 1223 K, alloy 1; △: 1293 K, alloy 1; ■: 1143 K, alloy 2; ●: 1223 K, alloy 2; ▲: 1293 K, alloy 2.

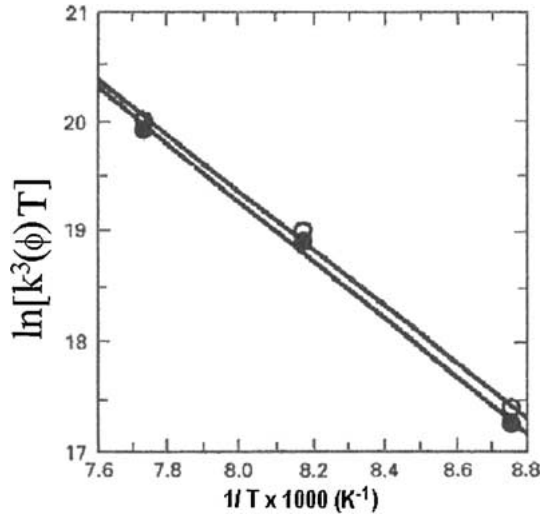

Figure 23 Arrhenius plot for determination of the activation energy for growth of γ' precipitates [21]. Key: ○: alloy 1, $Q = 272$ kJ mol^{-1}; ●: alloy 2, $Q = 277$ kJ mol^{-1}.

It was reported [153] that the study of Ni-Al-Mo-Ta and Ni-Al-Mo-W alloys indicated that γ' coarsening kinetics are in accordance with the LSW theory for the cube/ogdoad and rafted morphologies. In this study, values of activation energy for coarsening were 255 and 251 kJ/mole respectively for Ta-containing and W-containing alloys, which are rather close to the diffusion activation energy for Al in Ni, i.e. 269.2 kJ/mole [143]. In his study, Ardell [11] has determined the activation energy for coarsening of γ' in Ni-Al system to be approximately 269 kJ mol^{-1}, which is very close to the activation energy (269.2 kJ mol^{-1}) for diffusion of Al in very dilute Ni-Al alloys determined by Swalin

TABLE XI Activation energies for different nickel-base alloys

Alloy	Activation energy (kJ mole^{-1})	Source
Ni-Al	290.5	[32]
Ni-Al	262.5	[157, 173]
Ni-Al	277.8	[43]
Ni-Si	259	[11]
Ni-Ti	282.2	[122]
Ni-Al-Cr	358	[32]
Ni-Al-Mo-Ta	255	[151]
Ni-Al-Mo-W	251	[151]
Ni-Al-Cr-W-Mo-Ti	272	[21]
Ni-Al-Cr-W-Mo-Ti	277	[21]

and Martin [143]. However, a study of Ni-Al system by another worker [151] has shown that the activation energy for coarsening was rather high, i.e. 290.5 kJ/mole. Also, the activation energy [11] for coarsening of γ' in Ni-Si system is $\cong$259 kJ mol^{-1}, which is again almost identical to the activation energy for diffuson of Si in dilute Ni-Si alloys (257.9 kJ mol^{-1}) [150]. Table XI shows the results of activation energies for different alloying systems. Therefore, it is concluded that estimates of activation energy for coarsening of γ' particles in Ni-based superalloys have generally been approximately in the range of 250 to 290 kJ/mole, which are rather comparable to that for diffusion of alloying elements in Ni. In conclusion, γ' coarsening is a diffusion-controlled process. It is believed that differences in activation energies for coarsening of γ' precipitate particles are due to such factors as alloying compositions, scatters in experimental results, interactions between alloying elements, and different methods used for the evaluations of the data.

Another important useful parameter determined from the γ' coarsening experiments in Ni-based superalloys is the interfacial energy (Ψ_{int}). There has been less agreement in estimates of interfacial energy, with values ranging from 0.0089 to 0.0 37 kJ m^{-2} [22, 121, 19, 152]. A theoretical calculation by Williams [174] gave a value of 29 mJ m^{-2}, which agrees fairly well with the experiments.

Marsh and Chen [157] have also predicted the interfacial energy between the γ'–γ system in Ni-12.5 at.% Al alloy at different temperatures, using Equation 51. The results for the interfacial energy along with those of the other works are shown in Table X. The scatter in the data were attributed [157] to the differing compositions of Ni-Al represented as well as, possibly, a certain lack of precision inherent in applying the LSW theory to the analysis. Nevertheless, there is a tendency in the data overall which suggests a decrease in the precipitate-matrix interfacial energy as the temperature increases. One explanation for this would be the greater thermal expansion coefficient of the matrix compared to the precipitate [175]. This would lessen the interfacial misfit and so the associated elastic strain energy [157].

7.2. Shape changes and splitting in γ' particles

Elastically induced particle shape transitions are well known to occur in two-phase coherent alloys. In cubic materials, these transitions range from those that are symmetry conserving (in the sense that the particles retain the symmetry of the intersection of the point groups of the particles and matrix phases), such as the sphere-to-cube transition [96, 156], to those that are symmetry breaking, such as the sphere-to-ellipsoid or cube-to-cuboid transitions [7, 94]. Westbrook [53], Miyazaki *et al.* [33] and Doi *et al.* [34] have also identified a different type of transition, in which an isolated particle splits or fissions into two or more smaller particles. These transitions can be understood qualititatively in terms of the competition between the interfacial and elastic energies [7, 33, 34, 85, 94, 96, 176]. In these cases, the decrease in the elastic energy resulting from the transition more than compansates for the accompanying increase in the interfacial energy.

The first theoretical treatment of rafting was formulated by Tien and Copley [12] who used a purely thermodynamic argument to predict shapes that precipitates would assume in a stressed sample. Their qualitative calculations showed that precipitates with a smaller lattice parameter and elastic modulus than that of the matrix can lower the energy of a sample by forming plates perpendicular to an applied tensile stress. In contrast, they predicted that compressive stress would cause plates to form parallel to the applied stress. Their theoretical work was supported by actual experiments upon Udimet 700, a commercial superalloy in which they believed the γ' phase have a lower modulus than γ matrix. It is important to note that Tien and Copley did not consider crystal anisotropy or interparticle interactions in explaining directional coarsening. Their ability to develop a satisfactory qualitative explanation without considering these factors suggested that rafts could form by the response of individual particles to applied loads. Thus, it appeared that interparticle interactions were not necessarily important in this alloy, which contained a relatively low volume-fraction (39%) of γ'.

The next major advance in understanding rafting came from Pineau [53]. Pineau, too, ignored interparticle interactions and anisotropy, but made a more-sophisticated analysis of elastic energies. Specifically, he considered elastic-energy terms arising from three sources: lattice-parameter mismatch, differences in modulus between matrix and precipitate, and interactions between applied stress and coherency stresses. Microstructure were predicted by calculating elastic energies for three different shapes: spheres, needles parallel to the applied stress, and plates perpendicular to the stress. Pineau made quantitative predictions indicating that stress-level as well as direction of stress can affect the preferred direction of coarsening. In particular, Pineau predicted that precipitates with lower Young's modulus than that of the matrix will always form plates if the quantity σ_a/δ is positive, where σ_a is the applied stress (tension-positive values) and δ is lattice-parameter mismatch (positive when γ' has the larger lattice-parameter). In contrast, negative values of σ_a/δ would produce needle-shaped precipitates parallel to the stress axis at low stress levels, while higher stresses would produce plates perpendicular to the stress. These predicted effects of stress-magnitude apparently explained a discrepancy between the results

of Tien and Copley [12] and unpublished work of Carryy and Strudel [65]. Pineau also calculated that particle dimensions had to exceed a certain minimum size before rafting would occur. The minimum size was predicted to decrease with increasing stress.

Miyazaki *et al.* [14] continuing the efforts to explain rafting through elastic-energy considerations, considered effects of anisotropy. These authors predicted shapes of precipitates in Ni-15 at.% Al stressed along the [001] axis. They predicted that platelike precipitates would form in all stress conditions (tension, compression, or unstressed); however, the stress-state would affect orientation of the plates. Tension was predicted to induce plates parallel to the applied stress, while compression would cause the plates to form perpendicular to the stress. These predictions were contrary to those of Tien and Copley [12] and Pineau [53] but were consistent with Miyazaki *et al.*'s own experimental results. One important feature of Miyazaki *et al.*'s work was that it produced experimental evidence for the importance of interparticle interactions: during compressive loading, the precipitates formed rods as an unexpected intermediate stage of plate-formation. Rods are unstable with respect to plates, but they apparently form more rapidly. Miyazaki *et al.* suggested that they could do so because the precipitates naturally align themselves along ⟨001⟩ directions. Thus, rods might form more rapidly by coalescence along the rows, whereas plate-formation would require coalescence in two dimensions.

A different view about the rafting was provided by Carry and Strudel [65, 89] who considered the effects of plastic deformation by postulating the special dislocation arrangement between the γ/γ' interfaces located horizontal or vertical direction. They predicted precipitate shapes on the basis of whether the mobile dislocations would reduce misfit stresses preferentially on vertical or horizontal γ/γ' interfaces. It was assumed that γ' has a smaller lattice parameter. Therefore, mobile dislocations at the vertical interfaces would increase the local stress. Hence, the γ' precipitate particles were expected to form rods as the horizontal interfaces advanced at the expense of the vertical ones. Diffusional transport of γ'-forming elements between interfaces would, of course, be enhanced by the dislocation that connected them.

As the above discussion shows, various authors reach contrary conclusions both in their theories and in their experimental results. One possible explanation of these discrepancies is the controversy over the relative moduli of γ and γ', though modulus is irrelevant to Carry and Strudel's [65] model. Tien and Copley [12] and Pineau [53] used elastic constants for Ni_3Al and pure Ni, from which they concluded that γ should have the higher modulus. Miyazaki *et al.* [14] actually measured the modulus of γ in their Ni-Al binary alloy, and found that γ' had the higher modulus. However, Fisher [177] responded to Miyazaki *et al.* with data showing that γ' has a lower modulus in the Ni-Al binary system.

Lattice-mismatch measurements may be another source of disagreement among authors, since mismatch changes with temperature. The importance of this effect is now well recognized [37, 64, 178] but the theoretical

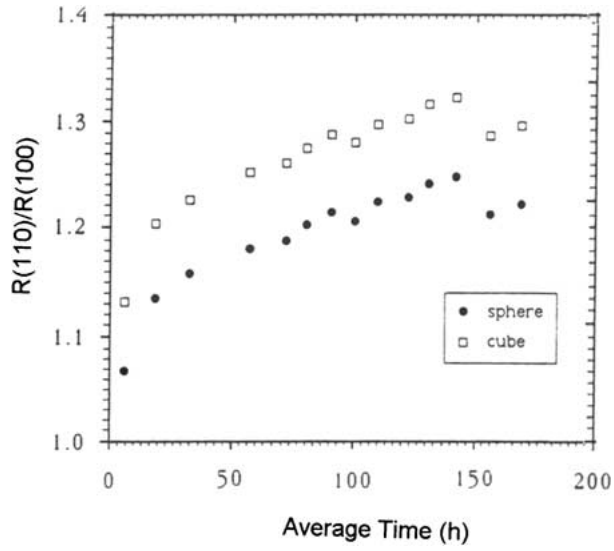

Figure 24 The ratio of the average size of the precipitate in two crystallographic directions [i.e., $R(110)/R(100)$] versus time at 675°C [157].

works discussed above have apparently not yet been reconsidered in the light of it. A through theoretical treatment of rafting would also have to consider elastic interactions between particles. Johnson's [93] work provides a basis for such an effort, but also suggests the theoretical difficulties posed by variations in particle shape. In particular, Johnson showed that particle-shape can affect both the sign and the magnitude of interaction energies. Thus, it is conceivable that an alloy might not raft if its γ' were spherical, for example, but would if it were aged to make the γ' cubic.

Marsh and Chen [157] has studied the shape changes of the γ' particles along the ⟨110⟩ and ⟨100⟩ directions during the precipitation reaction of a supersaturated solid solution single crystal of Ni-12.5 at.% Al alloy at moderately high temperatures using an *in situ* X-ray diffraction technique. Fig. 24 shows the ratio of the average precipitate dimensions along both the ⟨110⟩ and the ⟨100⟩ directions. For perfect spheres this ratio should be constant and equal to unity. For perfect cubes this ratio should be constant and equal to 1.414. Instead the ratio is seen to gradually increase within the range between these two values indicating that the morphology transition of sphere to cube is ongoing during coarsening.

It is well known that the morphology of coherent precipitates in two-phase alloys is strongly influenced by the elastic energy associated with the misfit between the precipitate and matrix structures. The reason is that the elastic energy depends on the shape, habit plane configuration of the precipitates, and as well as their volume. The shape dependence of the elastic energy is treated in the original work of Eshelby [8, 58, 74]. The preferred shape and habit are determined by the requirement that the sum of the elastic and surface energies be a minimum. The shape and habit that minimize the elastic energy depends on the elastic anisotropy of the system, which can be expressed in terms of the anisotropy factor: $A = C_{11} - C_{12} - 2C_{44}$, where the C_{ij} are the cubic elastic constants. The Ni_3Al phase has negative

anisotropy. For such precipitates the elastic energy is minimized when the precipitates has the form of an arbitrarily thin plate with a (100) habit. If the surface tension is isotropic, as it seems to be to reasonable approximation in most cubic systems, the progression of the preferred shape during coarsening is from a sphere to a cube bounded by (100) planes to a plate with a (100) habit that progressively thins as coarsening continues.

Kachaturyan *et al.* [96] have theoretically analyzed the strain induced shape changes in coarsening cubic shape precipitate particles and have made the following predictions: (a) Sphere $\rightarrow$ Cube if $2a_o \geq 7.7r_o$; (b) Cube $\rightarrow$ Doublet if $2a_o \geq 27r_o$; (c) Doublet $\rightarrow$ Octet if $2a_o \geq 82r_o$; (d) Octet $\rightarrow$ Plate if $2a_o \geq 377r_o$. Where $2a_o$ is the particle size before shape change, r_o is the Ψ_{int}/E_1 ratio and E_1 is the elastic energy per unit volume. Transition size is sensitive to the value of the interfacial energy between the particles and matrix. Splitting occurs when the cubic shape attains. Based upon the above-mentioned criteria shape changes of γ' particles in Ni-Al and Ni-Al-Cr systems were investigated, and as a result no transition of the shapes was possible [151]. It was suggested [151] that if splitting of particles does occur during coarsening, a discontinuous variation in the $\bar{a}^3$ with t (instead of a linear increase) would be expected. However, the $\bar{a}^3$ versus t plots did not show such behaviour.

It was observed that during the coarsening of coherent γ' precipitates, a single γ' particle sometimes splits into a group of eight small cuboids (i.e. an ogdoad) (see Fig. 8a) or into a pair of parallel plates (i.e. a doublet) [30, 33, 41]. This type of splitting is a typical example which indicates the importance of elastic interaction energy in determining the shape of individual γ' precipitates. The effects of elastic interaction energy on the shape might be described by the parameter Δ^*, the ratio of the γ–γ' lattice misfit to the surface energy of the γ' particles in the γ matrix ($\Delta^* = \delta/\psi_{int}$). The following three cases are observed according to the magnitude of Δ^*: (a) when $|\Delta^*| < 0.2$ the single γ' precipitate particles remain spherical and never split into several small particles, (b) when $0.2 < |\Delta^* < 0.4$ the single cuboidal γ' precipitate particles split into eight small cuboids (an ogdoad) and (c) when $0.4 \leq |\Delta^*|$ the single cuboidal γ' precipitate particles split into pairs of parallel plates (doublets).

References

1. A. BALDAN, *Z. Metallkde* **83** (1992) 324.
2. *Idem.*, *ibid.* **83** (1992) 331.
3. *Idem.*, *J. Mater. Sci.* **26** (1991) 3409.
4. *Idem.*, *ibid.* **30** (1995) 6288.
5. *Idem.*, *ibid.* **33** (1998) 3629.
6. T. MIYAZAKI, M. DOI and T. KOZAKAI, *Solid State Phenomena* **3/4** (1988) 227.
7. A. J. ARDELL and R. B. NICHOLSON and J. D. ESHELBY, *Acta Met.* **14** (1966) 1295.
8. J. D. ESHELBY, *Proc. R. Soc.* A **241** (1957) 376.
9. W. C. JOHNSON and J. K. LEE, *Metall. Trans.* **10A** (1979) 1141.
10. V. A. PHILIPS, *Acta Met.* **14** (1966) 1533.
11. A. J. ARDELL, in Proc. Int. Symp. On Mechanism of Phase Transformation in Crystalline Solids, Inst. of Metals Monograph and Report Series 33, 1968, p. 111.
12. J. K. TIEN and S. M. COPLEY, *Metall. Trans.* **2** (1971) 215.
13. *Idem.*, *ibid.* **2** (1971) 543.
14. T. MIYAZAKI, K. NAKAMURA and H. MORI, *J. Mater. Sci.* **14** (1979) 1827.
15. R. A. MACKAY and L. J. EBERT, *Metall. Trans.* **16A** (1985) 1969.
16. D. D. PEARSON, F. D. LEMKEY and B. H. KEAR, in Superalloys 1980, 4th Int. Conf. On Superalloys (ASM, Metals Park, OH, 1980) p. 513.
17. M. MC LEAN, *Metal Science* March (1978) 113.
18. N. S. STOLOFF, "Superalloys II" (John Wiley and Sons, New York, 1987).
19. D. MC LEAN, *Metal Sci.* **18** (1984) 249.
20. R. A. MACKAY and M. V. NATHAL, *Acta Metall. Mater.* **38** (1990) 993.
21. H. T. KIM, S. S. CHUN, X. X. YAO, Y. FANG and J. CHOI, *J. Mater. Sci.* **32** (1997) 4917.
22. A. J. ARDELL, *Acta Metall.* **20** (1972) 61.
23. C. K. L. DAVIES, P. NASH and R. N. STEVENS, *ibid.* **28** (1980) 179.
24. Y. ENOMOTO, M. TOKUYAMA and K. KAWASAKI, *ibid.* **34** (1986) 2119.
25. P. K. FOOTNER and B. P. RICHARDS, *J. Mater. Sci.* **17** (1982) 2141.
26. R. A. RICKS, A. J. PORTER and R. C. ECOB, *Acta Metall.* **31** (1983) 43.
27. S. B. FISHER and J. WHITE, *Mater. Sci. and Eng.* **33** (1978) 149.
28. R. A. STEVENS and F. FLEWITT, *ibid.* **37** (1979) 237.
29. J. SMITH, Ph.D. thesis, University of Illinois, Urbana-Champaign, 1987.
30. M. DOI and T. MIYAZAKI, in Proc. 5th Int. Symp. On Superalloys, Seven Springs, PA, October 1984, edited by M. Gell, C. S. Kortovich, R. H. Bricknell, W. B. Kent and J. F. Radevich (Metall. Soc. AIME, Warrendale, PA) p. 543.
31. T. MIYAZAKI, H. IMAMURA, H. MORI and T. KOZAKI, *J. Mater. Sci.* **16** (1981) 1197.
32. D. J. CHELMAN and A. J. ARDELL, *Acta Metall.* **22** (1974) 577.
33. T. MIYAZAKI, H. IMAMURA and T. KOZAKI, *Mater. Sci. and Eng.* **54** (1982) 9.
34. M. DOI, T. MIYAZAKI and T. WAKATSUKI, *ibid.* **74** (1985) 139.
35. M. CORNET and G. MARTIN, *Scripta Metall.* **21** (1987) 1091.
36. J. P. DENNISON, P. D. HOLMES and B. WILSHIRE, *Mater. and Eng.* **33** (1978) 35.
37. H. BURT, J. P. DENNISON, I. C. ELLIOT and B. WILSHIRE, *Mater. Sci.and Eng.* **53** (1982) 245.
38. J. PETERMAN, *Z. Metalkde* **62** (1971) 324.
39. J. W. CAHN and J. J. WEINS, unpublished work, Department of Metallurgy and Materials Science, MIT, Cambridge, MA.
40. G. SAUTHOFF, *Z. Metalkde.* **66** (1975) 106.
41. M. DOI, T. MIYAZAQUI and T. WAKATSUKI, *Mater. Sci. and Eng.* **67** (1984) 247.
42. D. D. PEARSON, B. H. KEAR and F. D. LEMKEY, in "Creep and Fracture of Engineering Materials and Structures," edited by B. Wilshire and D. R. Owens (Pineridge Press, Swansea, UK, 1981) p. 213.
43. T. B. GIBBONS and B. E. HOPKINS, *Metal Sci.* **18** (1984) 273.
44. P. CARON and T. KHAN, *Mater. Sci. and Eng.* **61** (1983) 173.
45. R. A. MACKAY and L. J. EBERT, in Proc. 5th Int. Symp. On Superalloys 1984, edited by M. Gell, C. S. Kortovich, R. H. Bricknell, W. W. Kent and J. F. Radovich, Metallurgical Society of AIME, Warrendale, PA, 1984 p. 135.
46. M. MCLEAN, in Proc. Conf. On Advanced Materials and Processening Techniques for Structural Applications, Paris, September 7–9, 1987, edited by T. Khan and A. Lasalmonie, ONERA.
47. M. I. NATHAL and L. J. EBERT, *Scripta Metall.* **17** (1983) 1151.
48. R. A. MACKAY and L. J. EBERT, *ibid.* **17** (1983) 1217.
49. M. FELLER-KNIEPMEIER and T. LINK, *Metall. Trans.* A **20A** (1989) 1233.
50. J. GAYDA and R. A. MACKAY, *Scripta Metall.* **23** (1989) 1835.

51. T. M. POLLACK and A. S. ARGON, *Acta Metall. Mater.* **42** (1994) 1859.
52. J. M. OBLAK, D. F. PAULONIS and D. S. DUVALL, *Metall. Trans.* **5**(1974) 143.
53. A. PINEAU, *Acta Metall.* **24** (1976) 559.
54. W. C. JOHNSON, *ibid.* **32** (1984) 465.
55. M. DOI, *Mater. Trans., JIM* **33**(1992) 637.
56. Y. WANG and A. G. KHACHATURYAN, *Acta Metall. Mater.* **43** (1995) 1837.
57. J. K. LEE, *Metall. Mater. Trans.* **27A** (1996) 1449.
58. J. D. ESHELBY, *Proc. R. Soc.* A **242**(1959) 561.
59. J. GAYDA and D. J. SROLOVITZ, *Acta Metall.* **37** (1989) 641.
60. J. L. VALLES and D. J. ARRELL, *Acta Metall. Mater.* **42** (1994) 2999.
61. H. NISHIMORI and A. ONUKI, *Phys. Rev.* B **42** (1990) 980.
62. D. Y. LI and L. Q. CHEN, *Scripta Metall.* **37** (1997) 1271.
63. F. R. N. NABARRO, *ibid.* **37** (1997) 497.
64. A. FREDHOLM and J. L. STRUDEL, in Proc. 5th Int. Symp. on Superalloys, Champion, PA, October 7–11, 1984, edited by M. Gell, C. S. Kortovich, R. R. Bricknell, W. B. Kent and J. F. Radovich (1984) p. 211.
65. C. CARRY and J. L. STRUDEL, *Acta Metall.* **26** (1978) 859.
66. G. R. LEVERANT, B. H. KEAR and J. M. OBLAK, *Metall. Trans.* **4** (1973) 355.
67. I. L. STEVTLOV, B. A. GOLOVKO, A. I. EPISHIN and N. P. ABALAKIN, *Scripta Metal. Mater.* **26** (1992) 1353.
68. Z. F. PENG, U. GLETZEL and M. FELLER-KNIEPMEIR, *Acta Metall. Sin* A **31** (1995) A533.
69. *Idem.*, *Scripta Mater.* **34** (1996) 221.
70. S. G. TIAN, H. H. ZOU, J. H. ZHANG, H. C. YAN, Y. B. XU and Z. O. HU, *Mater. Sci. Eng.* **16** (2000) 451.
71. M. VERON, Y. BRECHET and F. LOUCHET, in "Superalloys 1996" (TMS/AIME, Warrendale, PA, 1996) p. 181.
72. F. R. N. NABARRO, *Metall. Trans.* A **27A** (1996) 513.
73. F. R N. NABARRO, C. M. CRESS and P. KOTSCHY, *Acta Metall.* **44** (1996) 3189.
74. J. D. ESHELBY, *Prog. Solid Mech.* **2** (1961) 89.
75. J. K.LEE, D. M. BARNETT and H. I. AARONSON, *Metall. Trans.* A **8A** (1977) 963.
76. A. G. KHACHATURYAN and G. A. SHATALOV, *Soviet Phys. Solid Stat.* **11** (1969) 118.
77. L. M. BROWN, R. H. COOK, R. K. HAM and G. R. PURDY, *Scripta Metall.* **7** (1973) 815.
78. A. G. KHACHATURYAN and G. A. SHATALOV, *Phys. Stat. Sol.* (a) **26** (1974) 61.
79. V. PEROVIC, G. R. PURDY and L. M. BROWN, *Acta Metall.* **27** (1979) 1075.
80. A. G. KHACATURYAN, *Sov. Phys., Solid Stat.* **8** (1967) 2163.
81. E. SEITZ and D. DE FOUNTAINE, *Acta Metall.* **26** (1978) 1671.
82. J. K. LEE and W. C. JOHNSON, *Scripta Metall.* **11** (1977) 477.
83. J. D. ESHELBY, *Ann. Phys.* **7** (1958) 116.
84. F. V. NOLFI, *J. Appl. Phys.* **47** (1976) 24.
85. W. C. JOHNSON, *Acta Metall.* **32** (1984) 465.
86. K. TANAKA, T. MORI and T. NAKAMURA, *Phil. Mag.* **21** (1970) 267.
87. K. ROBINSON, *J. Appl. Phys.* **22** (1951) 1045.
88. W. LOOMIS, J. FREEMAN and D. SPONSELLER, *Metall. Trans.* **3** (1972) 989.
89. C. CARRY and J. L. STRUDEL, *Acta Metall.* **25** (1977) 767.
90. W. BOAS and J. K. MACKENZIE, *Prog. Met. Phys.* **2** (1950) 90.
91. J. K. LEE and W. C. JOHNSON, *Phys. Sol. Stat.* (a) **46** (1978) 267.
92. G. IOOS and D. D. JOSEPH, "Elementary Stability and Bifurcation" (Springer, Berlin, 1980) Ch. 1.
93. W. C. JOHNSON, *Metall. Trans.* **14A** (1983) 2219.
94. *Idem.*, *Acta Metall.* **32** (1984) 1925.
95. T. MIYAZAKI, H. IMAMURA and T. KOZAKAI, *J. Mater. Sci.* **54** (1982) 9.
96. A. G. KHACHATURYAN, S. V. SEMENOVSKAYA and J. W. MORRIS, *Acta Metall.* **36** (1988) 1563.
97. C. WAGNER, *Z. Elektrochem.* **65** (1961) 581.
98. G. W. GREENWOOD, *Acta Metall.* **4** (1956) 243.
99. I. M. LIFSHITZ and V. V. SLYOZOV, *J. Phys. Chem. Solids* **19** (1961) 35.
100. K. HARRIS, G. L. ERIKSON and R. E. SCHWER, "Metals Handbook, Vol. 1: Properties and Selection," 10th ed. (ASM International, Materials Park, OH, 1989) p. 581.
101. T. MIYAZAKI, K. SEKI, M. DOI and T. KOZAKAI, *Mater. Sci. Eng.* **77** (1986) 125.
102. W. C. JOHNSON, P. W. VOORHEES and D. E. ZUPON, *Metall. Trans.* **20A** (1989) 1175.
103. P. W. VOORHEES, G. B. MACFADDEN and W. C. JOHNSON, *Acta Metall. Mater.* **11** (1992) 2979.
104. A. B. BRAILSFORD and P. WYNBLATT, *Acta Metall.* **27** (1979) 489.
105. P. W. VOORHEES and M. E. GLICKSMAN, *ibid.* **32** (1984) 2001, 2013.
106. K. TSUMARAYA and Y. MIYATA, *ibid.* **31** (1983) 437.
107. R. ASIMOV, *ibid.* **11** (1963) 72.
108. R. W. HENKEL, *Trans. Metal. Soc. AIME* **233** (1965) 1994.
109. S. SARIN and H. W. WEART, *J. Appl. Phys.* **37** (1966) 1675.
110. P. NASH, *Scripta Metall.* **18** (1984) 295.
111. K. TSUMARAYA, *ibid.* **18** (1984) 297.
112. J. A. MARQUSEE and J. ROSE, *J. Chem. Phys.* **79** (1983) 373.
113. *Idem.*, *ibid.* **80** (1984) 536.
114. G. VENZEL, *Phys. Rev.* A **32** (1985) 3431.
115. M. TOKUYAMA and K. KAWASAKI, *Physica* **123A** (1984) 384.
116. P. W. VOORHEES, *J. Stat. Phys.* **38** (1985) 231.
117. A. J. ARDELL and R. B. NICHOLSON, *J. Phys. Chem. Solids* **27** (1966) 1993.
118. V. BISS and D. SPONSELLER, *Metall. Trans.* **4** (1973) 1953.
119. A. J. ARDELL, *Acta Metall.* **16** (1968) 511.
120. O. H. KRIEGE and J. M. BARIS, *Trans. ASM* **62** (1969) 195.
121. A. J. ARDELL, *Metall. Trans.* **1** (1970) 525.
122. E. HORNBOGEN and M. ROTH, *Z. Metallkde* **58** (1967) 824.
123. B. A. PARKER and D. R. F. WEST, *Australian Inst. of Metals* **14** (1969) 102.
124. W. I. MITCHELL, *Z. Metallkde* **57** (1966) 586.
125. T. MUKHERJEE, W. E. STUMPF, C. M. SELLARS and W. J. MCTEGART, *J. Iron and Steel Inst.* **207** (1969) 621.
126. P. K. MADDEN and V. M. CALLEN, *J. Mater. Sci.* **18** (1983) 3363.
127. R. J. WHITE and S. B. FISHER, *Mater. Sci. Eng.* **33** (1978) 149.
128. V. RANDLE and B. RALPH, *Acta Metall.* **34** (1986) 891.
129. *Idem.*, *Mater. Sci. Eng.* **3** (1987) 411.
130. A. A. HOOPGOOD and J. W. MARTIN, *ibid.* **2** (1986) 543.
131. H. HIRATA and D. H. KIRKWOOD, *Acta Metall.* **25** (1977) 1425.
132. H. GLEITER and E. HORNBOGEN, *Z. Metallkde.* **58** (1967) 157.
133. P. HENDERSON and M. MC LEAN, *Acta Metall.* **31** (1983) 1203.
134. E. H. MOLEN, T. M. OBLAK and D. H. KRIEGE, *Metall. Trans.* **2** (1971) 1627.
135. P. K. MADDEN and V. M. CALLEN, *J. Mater. Sci.* **18** (1983) 3367.
136. H. WENDT and P. HAASEN, *Acta Metall.* **31** (1983) 1649.
137. A. W. THOMSON and J. A. BROOKS, *ibid.* **31** (1982) 2197.
138. K. B. S. RAO, V. SEETHARAMAN, S. L. MANNAN and P. RODRIGUEZ, *Mater. Sci. Eng.* **58** (1983) 93.
139. H. G. BRION and E. NEMBACH, *Phys. Stat. Sol.* (a) **26** (1974) 599.
140. B. MCGURRAN and J. W. MARTIN, *Z. Metallkde.* **72** (1981) 538.
141. R. E. BEDDOE, P. HAASEN and G. KOSTORZ, *ibid.* **75** (1984) 213.
142. E. NEMBACH and G. NEITE, *Prog. Mater. Sci.* **29** (1985) 177.
143. R. A. SWALIN and A. MARTIN, *J. Metals* **8** (1956) 567.
144. A. GES, O. FORNARO and H. PALACIO, *J. Mater. Sci.* **32** (1997) 3687.
145. P. K. RASTOGI and A. J. ARDELL, *Acta Metall.* **19** (1971) 321.
146. A. J. ARDELL, *ibid.* **15** (1967) 1772.

147. C. S. JAYANT and P. NASH, *J. Mater. Sci.* **24** (1989) 3041.
148. R. A. ORIANI, *Acta Metall.* **12** (1964) 1399.
149. A. J. ARDELL, in Phase Transformations' 87, Inst. of Metals Proc. 1987 (University of Cambridge, 1988) p. 485.
150. R. W. SWALIN, A. MARTIN and R. OLSEN, *Trans. Am. Inst. Min. Met. Eng.* **209** (1957) 936.
151. C. S. JAYANT and P. NASH, *Mater. Sci. Tech.* **6** (1990) 405.
152. C. K. L. DAVIES, P. NASH and R. N. STEVENS, *J. Mater. Sci.* **15** (1980) 1521.
153. S. SADIQ and D. R. F. WEST, *Scripta Metall.* **19** (1985) 833.
154. M. VITTORI, *J. Mater. Sci.* **16** (1981) 3461.
155. YE-FANG HUN, P. DEB and M. C. CHATURVEDI, *Metal Sci.* **16** (1982) 555.
156. M. E. FINE, J. R. WEERTMAN and J. G. CONLEY, in Phase Transformations' 87, Proc. of Conf., held at the University of Cambridge, 6–10 July 1987, edited by G. W. Lorimer, p. 501.
157. C. MARSH and H. CHEN, *Acta Metall.* **38** (1990) 2287.
158. R. KAMPMANN and R. WAGNER, in Decomposition of Alloys: The Early Stages, Proc. of Sonnenberg, Germany (1983) p. 91.
159. M. HANSEN, "Constitution of Binary Alloys" (McGraw-Hill, New York, 1958).
160. A. TAYLOR and R. W. FLOYD, *J. Inst. Metals* **81** (1952) 25.
161. P. K. RASTOGI and A. J. ARDELL, *Acta Metall.* **17** (1969) 595.
162. C. Y. LI and R. A. ORIANI, "Oxide Dispersion Strengthening," Metall. Soc. Conf., Vol. 431 (Gordon and Breach, New York, 1968) p. 431.
163. R. E. HOFFMAN, F. W. PIKUS and R. A. WARD, *J. Metals* **8** (1956) 483.
164. H. W. ALLISON and H. SAMELSON, *J. Appl. Phys.* **30** (1959) 1419.
165. T. YAMAMOTO, T. TAKASHIMA and K. NISHIDA, *Trans. Japan Inst. Metals* **21** (1980) 601.
166. A. R. WAZZAN, *J. Appl. Phys.* **36** (1965) 3506.
167. M. FELLER-KNIEPMEIR, M. GRUNDLER and H. HELFMEIR, *Z. Metallk.* **67** (1976) 533.
168. J. E. DORN, *Trans. Am. Soc. Metals* **53** (1961) 227.
169. W. GUST, M. B. HINTZ, A. LODDING, H. ODELIUS and B. PREDEL, *Phys. Stat. Sol.* (a) **64** (1981) 183.
170. S. Q. XIAO, P. J. WILLBRANDT and P. HAASEN, *Scripta Metall.* **23** (1989) 295.
171. G. R. LEVERENT, B. H. KEAR and J. M. OBLAK, *Metall. Trans.* **4** (1973) 355.
172. P. NASH, Ph.D. thesis, University of London, 1977.
173. A. F. GIAMEI and D. L. ANTON, *Metall. Trans.* A **16A** (1985) 1977.
174. R. O. WILLIAMS, *Trans. AIME* **215** (1959) 1026.
175. M. P. ARBUZOV and I. A. ZELENKOV, *Fizika Metall. Metallov.* **16** (1963) 236.
176. J. H. WESTBROOK, *Z. Kristallog.* **110** (1958) 21.
177. E. S. FISHER, *Scripta Metall.* **20** (1986) 279.
178. D. H. GROSS and G. S. ANSELL, *Metall. Trans.* A **12A** (1981) 1631.

Received 5 March 2000
and accepted 19 December 2001